



## MATERIALS & METHODS

# Which forces acts on centrosome separation?

*Fabio Echegaray, Thomas Stiff, Helfrid Hochegger*

# 1 Materials & Methods

## 1.1 Capturing Centrosome Dynamics in G2/M Phase Through Immunofluorescence Microscopy

**Base cell line and live cell imaging experiments** The assay for measuring centrosome positioning forces has already been well established in the lab and has been conducted mainly by Dr. Thomas Stiff. We use a U2OS cell line that expresses a Cdk1 analogue sensitive mutation. This allows the tight and specific inhibition of Cdk1 by the addition of the small molecule 1NMPP1. This results in a prolonged G2 arrest during which centrosomes separate due to the action of Plk1 and Eg5 motors. Inhibition of Eg5 causes rapid congression of the centrosomes due to the positioning force mechanism. Thus, measuring the dynamics of this movement allows a simple estimation of the generated net force that impacts on the centrosomes. To perform these measurements the U2OS cells stably express beta-tubulin-GFP and RFP-PACT domain that allows visualisation of the centrosome and perform live cell immunofluorescence microscopy.

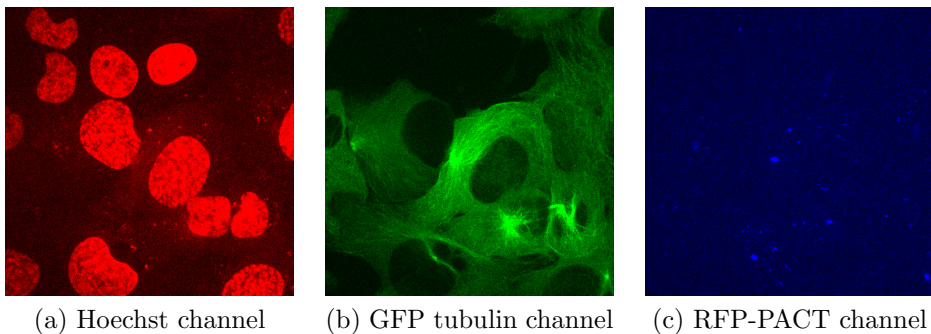


Figure 1: Image channels available to processing for centrosome tracking.

To track centrosomes movement relative to the nuclear centroid, we segmented the nucleus and centrosomes based on Hoechst 33342 and RFP-PACT staining. Figure 1 show an example of each channel. At the moment, we're only processing the Hoechst and RFP channels, and I'm currently working on using the information that's contained in the GFP-tubulin channel to make an estimation of the cell shape and to characterize the microtubule network.

Tracking was performed using TrackMate plugin from ImageJ. We needed to extract centrosome position, and nuclei centroid coordinates in order to reference centrosomes to a particular nuclei, and the corresponding nuclei to

the image coordinate system (ICS).

For the RFP channel -centrosome position tracking-, we applied a threshold on the output image and remove some noise, then detected particles using the Laplacian of gaussian (LoG) transform, tracked them using a Kalman Filter, and finally extracted candidates by filtering the output based on track lengths and gaps criteria.

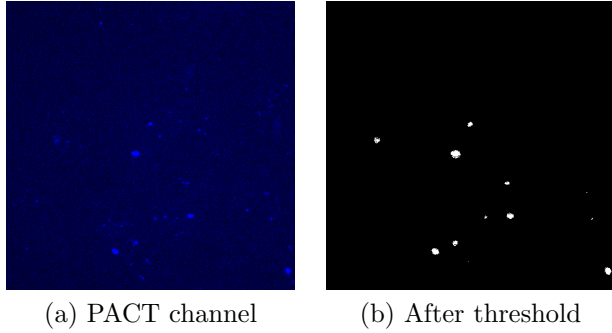


Figure 2: Image processing for PACT channel

We had some complications in order to get a good measure of the nuclear centroid in the Hoechst channel. For that matter, we applied a series of steps in order to get an estimate of it. Figure 3 shows an example of the output at each step of the segmentation algorithm, which takes place in the following way:

1. A first threshold is applied to the image 3a.
2. Morphological close and open operations are done in the image to remove holes from chromosome condensation (figure 3c) and remove noise (fig 3d) respectively.
3. (3e) Distance transform is applied.
4. (3f) Gaussian blur is used as a low pass filter to soften out edges.
5. (3g) Second threshold is applied.
6. (3h) Watershed transform is used to cut two -probably- merged nuclei.

The output of the previous process is a set of blobs in the image, as can be seen in the figure 3h. We computed the centroid of the nuclear masks in each image using the method described in appendix ??, equation ??, and we

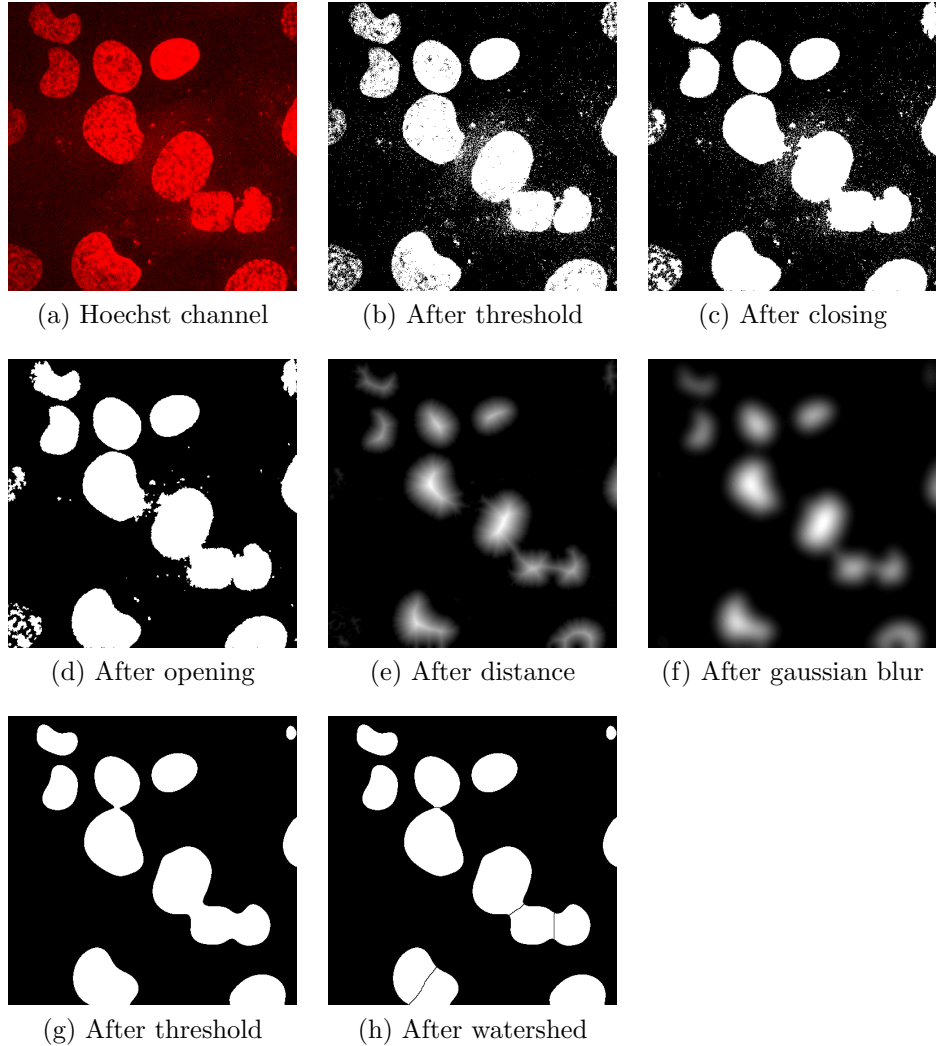


Figure 3: Image processing for the hoechst channel

reference the centrosome position relative to that point, according to figure 4, using the following equation

$$\begin{aligned}\vec{r}_{nc1} &= \vec{r}_{c1} - \vec{r}_n \\ \vec{r}_{nc2} &= \vec{r}_{c2} - \vec{r}_n\end{aligned}\tag{1}$$

Where vectors  $\vec{r}_{nc1}$  and  $\vec{r}_{nc2}$  are the position of each centrosome relative to nuclei centre, vector  $\vec{r}_n$  correspond to nucleus centroid and it's measured from the ICS,  $\vec{r}_{c1}$  and  $\vec{r}_{c2}$  position of first and second centrosome respectively, both measured from the ICS. The vectors  $\vec{r}_{nc1}$  and  $\vec{r}_{nc2}$  are not known *a priori*,

but can be fully obtained if we know the positions of the nucleus centre and each centrosome referenced to an arbitrary coordinate system.

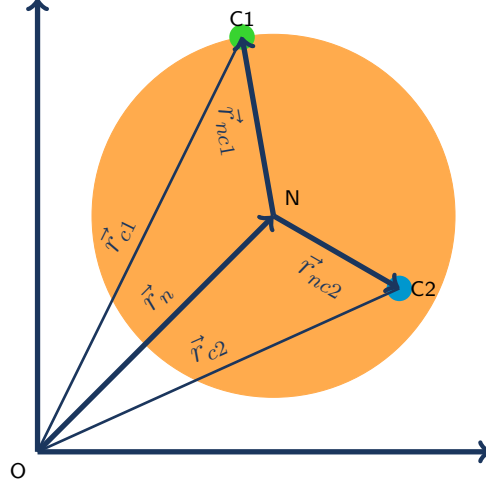


Figure 4: Nuclei and centrosome vectors.

Figure 5 shows an example of the algorithm output. We labelled centrosomes using yellow dots, the nuclei centre as a blue dot, and the nucleus boundary as a red curve. The relationship of centrosomes with the nucleus centre is represented by a white line. From these basic position measurements, we can obtain more sophisticated estimations. In particular, we were also interested in distance between centrosomes, speed towards nuclei, speed between centrosomes, and Mean square displacement (MSD), a measure of how much a centrosomes moves, which is explained in the appendix ???. Figure 6 shows an example of the first four measures based on the sequence shown in the previous figure.

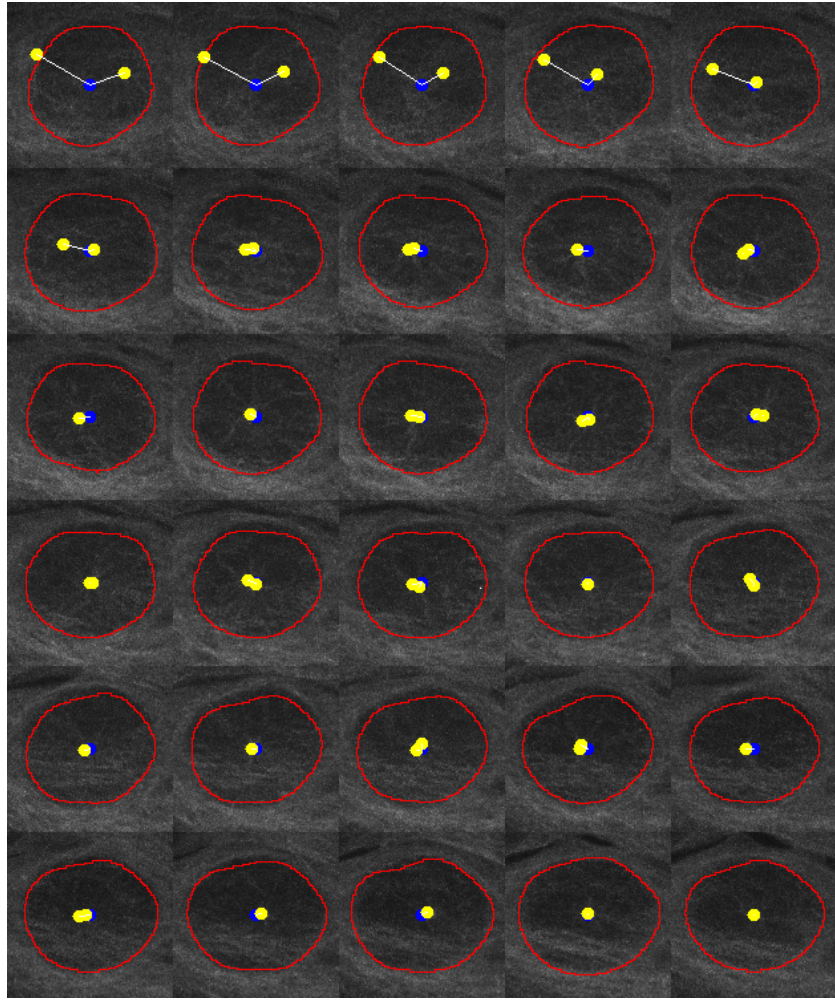


Figure 5: Output of the centrosome tracking algorithm. Yellow dots are centrosomes detected and referenced to the nuclei centre, draw as a blue dot. Red polygon correspond to the nucleus boundary.

### 1.1.1 Results

**Eg5 inhibition in G2 arrested cells causes centrosome congression towards the centre of the cell nucleus** It has been shown by previous research in our lab that inhibiting Eg5 in G2 cells with separated centrosomes causes rapid reversal of separation (13). This phenomena is going to be referred as *congression* from now on. To further analyse it, we tracked centrosomes in cells arrested in G2 with separated centrosomes that congressed following Eg5 inhibition by S-trityl-L-cysteine (STLC) (12). We can

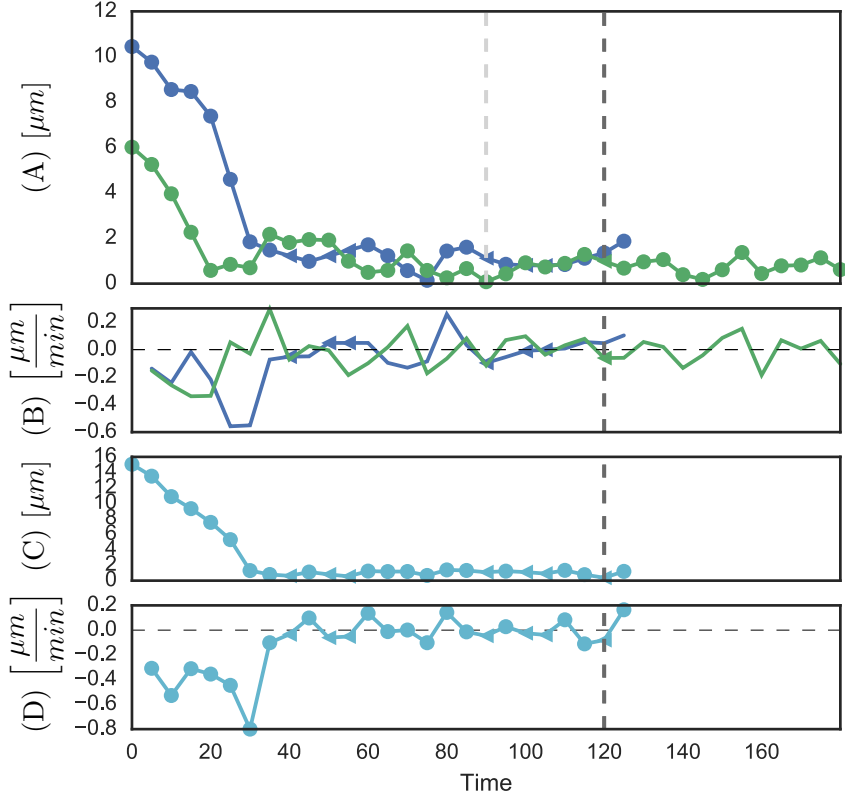


Figure 6: Measurements for the centrosomes the example figure 5. (A) corresponds to distance of each centrosome towards nuclei centre over time. (B) speed of each centrosome relative to nuclei centre. (C) distance between centrosomes. (D) speed between centrosomes. Dots and triangles represent measured and interpolated data respectively, vertical dark grey line represents contact time, and light grey 30 minutes before contact time.

observe in figure 7 the rapid centrosome congression after STLC addition, in contrast with cells with no STLC.

An interesting question for the +STLC group is how much time do centrosomes require to make contact. Although the answer to this question depends on the initial centrosome position for a given -absolute- time, one can measure the speed of the centrosome before contact and get an estimation on the rate which centrosomes approach each other. For this matter we define *time of contact* as follows

**Time of contact** Let  $d(t)$  be the distance between centrosomes over time,  $t = t_0, \dots, t_k \quad k \in \mathbb{N}$ . Then the *time of contact*  $t_c$  is the first element of the

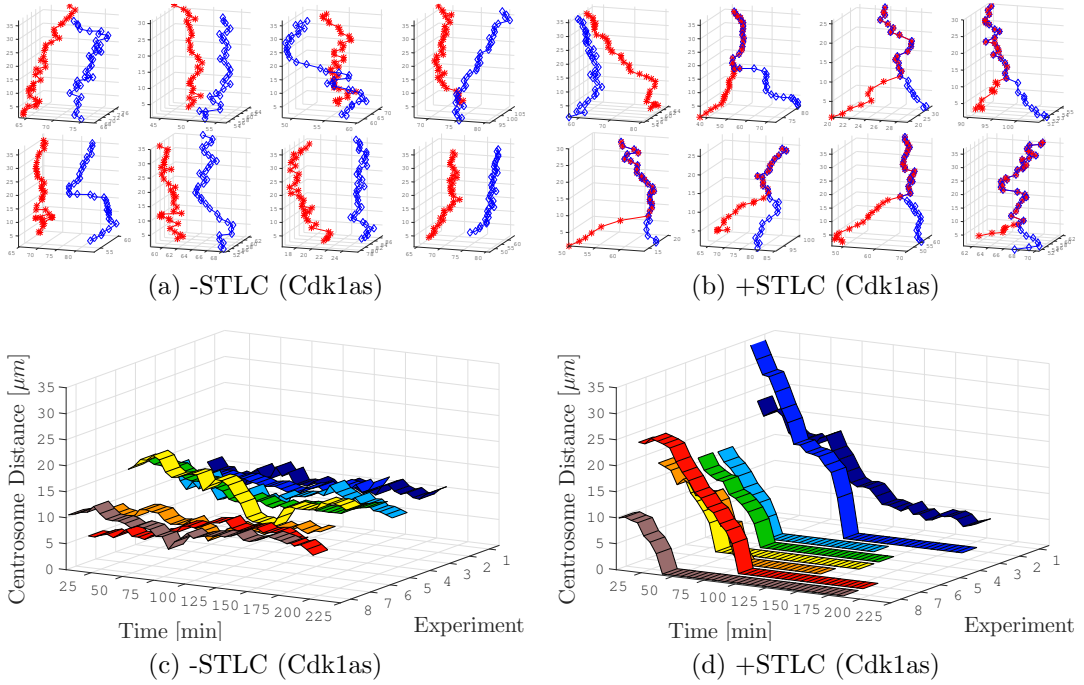


Figure 7: Impact of Eg5 inhibition on cells arrested in G2 phase. 7a shows example centrosome tracks for cells arrested in G2 phase. 7c shows distance over time for the previous tracks. 7b and 7d shows tracks and distance over time for cells arrested in G2 phase after Eg5 inhibition by STLC addition.

set

$$\{t_k \in \mathbb{R} : d(t_k) \leq d_{thr}\} \quad (2)$$

i.e.  $t_c = t_0$

We are currently using a threshold distance  $d_{thr} = 1.0[\mu\text{m}]$  to detect time of contact. We then define *contact speed* as the average speed of a centrosome until time of contact

$$v_{contact} = \frac{d(t_c)}{t_c} \quad (3)$$

When there's no congression, we let  $t_c = t_{max}$ . Differences in contact and instant speed for the two groups can be seen in figure 8. Instant velocity doesn't change considerably between the two groups, although they move faster after STLC addition. Contact velocity on the other hand shows a considerable difference between them. Estimation of the congression speed is approximately  $0.24 [\mu\text{m} \cdot \text{min}^{-1}]$ .

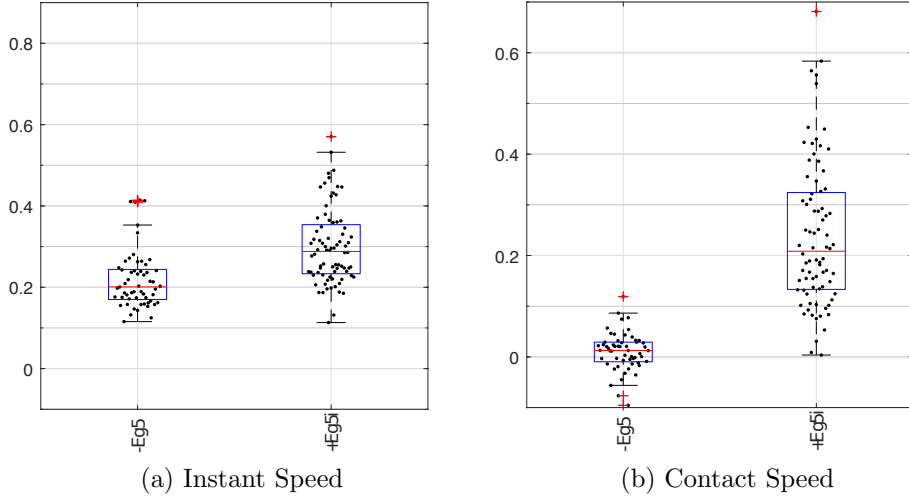


Figure 8: Contact and instant speed of cells arrested in G2 phase before and after Eg5 inhibition.

If we focus our attention to centrosome distance, we can see some interesting evidence. Figure 9 shows boxplots of distances towards nuclei and cell centre. At time of contact (figure 9.C), we observe that most of the centrosomes are very close to the nuclei centre, instead of the cell (figure 9.D), suggesting that there's a mechanism that moves the centrosomes towards the nucleus. This hypothesis is supported by the fact that 30 minutes before contact (9.A & 9.B) one centrosome is closer to the nuclei centre than the other, henceforth discarding a process that might be interacting on the centrosomes with the cell cortex or other structures, for example, interaction with just the microtubule network. Nuclear interaction becomes evident in the light of this data.

**Centrosome congression affects differentially the individual centrosomes** Data on 9.A and 9.B would also suggest different dynamics for the mother and daughter centrosome, as one is further away than the other. Pioneering work by (9) established that the mother centriole remains stably positioned in the cell centre during G1 phase and is more tightly interlinked with the cellular MT network than the daughter centriole. However, the authors observed that this difference was gradually lost during S-phase and that the two replicated centrosomes were indistinguishable in G2 phase. Our data on nuclei distance suggests something different. The fact that one cen-

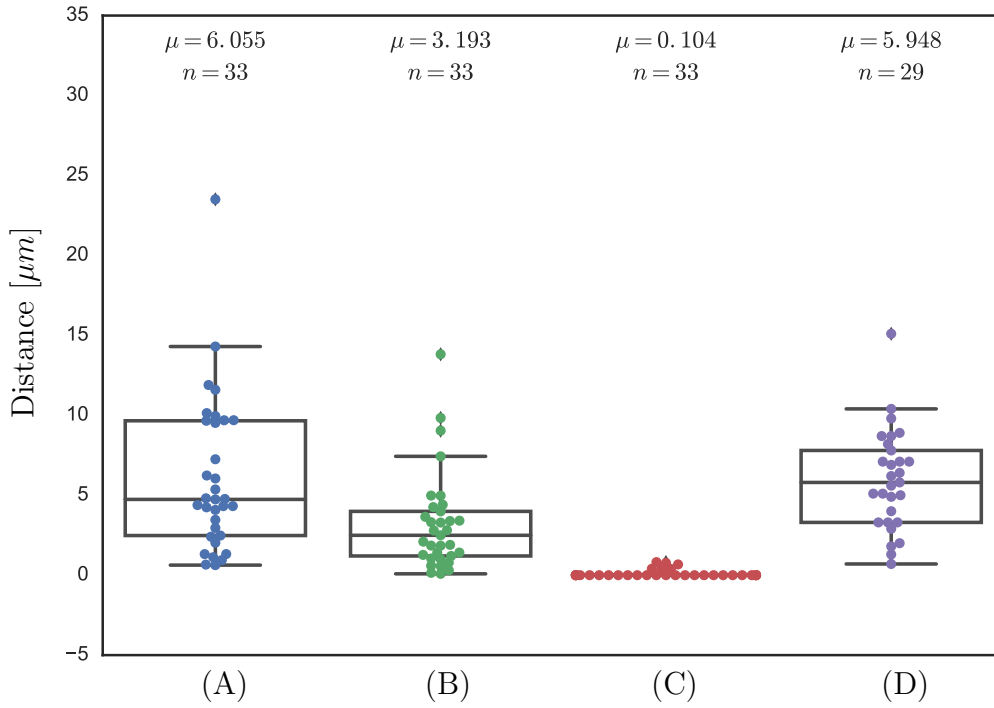


Figure 9: Centrosome distance of U2OS CDK1as cells in G2 arrest after STLC addition. (A) & (B) Centrosomes away from nuclei centre 30 minutes before contact. (C) Centrosomes from nuclei centre at time of contact. (D) Centrosomes from cell centre at time of contact.

tosome tends to be closer to the nucleus centre intrigued us. To further analyse this, we applied MSD analysis of each individual track.

MSD is a measure of the deviation of a particle from some reference position through time (also called delay), and its explained in appendix ???. We computed the MSD for each pair of centrosomes of each nucleus, characterising them in two groups, one where centrosomes move more, and a second where centrosomes move less, as shown in figures 10 and 11. Close observation of the tracks from both groups revealed a striking difference in displacement between the centrosome pairs following Eg5 inhibition, suggesting that one centrosome's motion is driven by a force, while the other is only moving in a diffusive way.

show msd D parameter and explain why it must be force driven

In fact, according to figure 12 -where both groups are compared together-after STLC addition there's a group that shows a non linear, increasing

convex mean MSD curve, implying there must be a force acting on that set of particles.

what's the MSD of the nucleus only, does it have the same coefficient that the centrome?

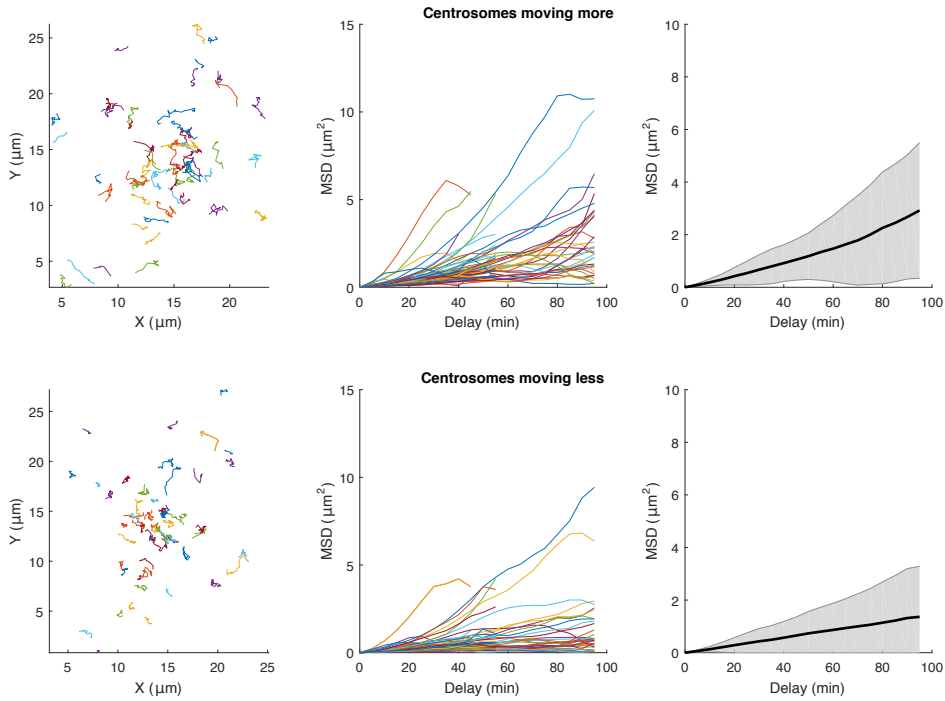


Figure 10: MSD for centrosomes of cells arrested in G2 by Cdk1 knock down with no Eg5 inhibitor

**Dynein role in centrosome congression** One of the forces that could be inflicted in the centrosomes is the indirect pulling of the Microtubule (MT) network by the motor Dynein. Having established the dynamics of centrosome positioning in G2 phase using the congression assay, we next tested the impact of this motor on the force generation mechanism and depleted two essential components of the multimeric cytoplasmic Dynein complex, Dynein heavy chain (DHC) and Dynein intermediate chain (DIC) in G2 arrested U2OS cells. Figure 13 shows examples of centrosome congression in Dynein depleted G2 arrested cells. At the onset of the experiment one or both of the centrosomes was significantly displaced from the nuclear envelope (NE) resulting in increased distance between the separated pair. Following Eg5 inhibition, the centrosomes moved steadily towards each other, but did appear to pause once they have reached the nuclear periphery. Ultimately,

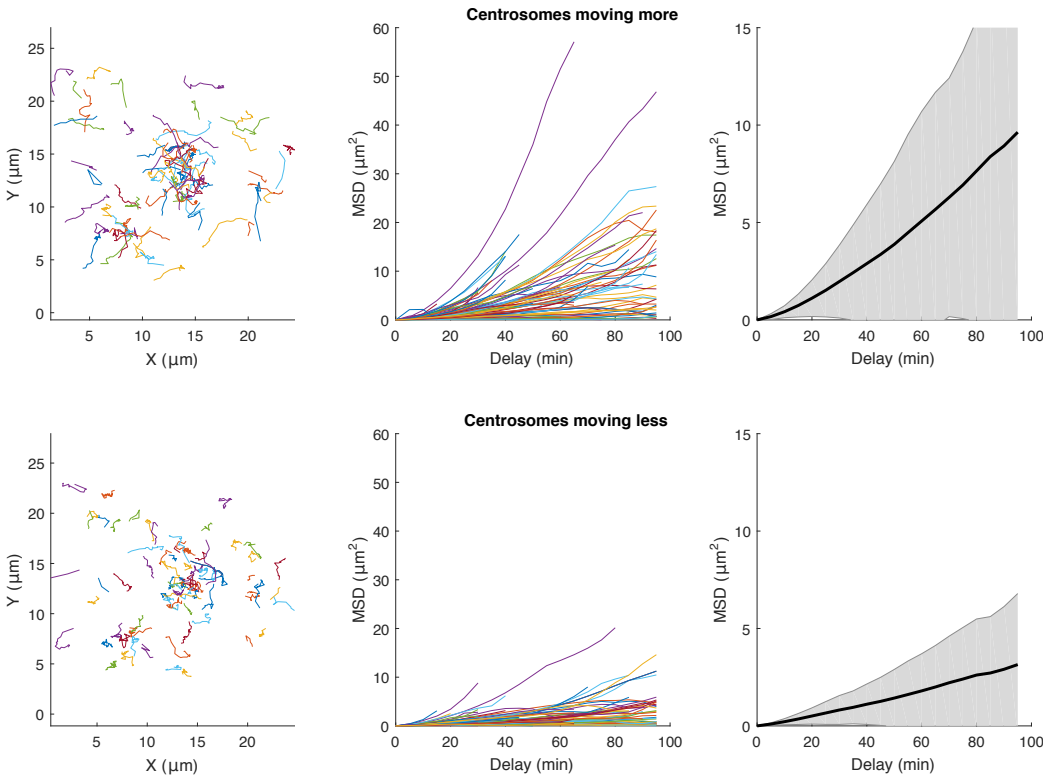


Figure 11: MSD for centrosomes of cells arrested in G2 after STLC addition

centrosomes mostly failed to meet each other within the course of the experiment. To quantify the dynamics of congression in the Dynein depleted cells, we compared the relative speed of centrosomes moving towards each other in Dynein depleted and control cells and plotted the average velocities over time, as well as scoring the percentage of centrosomes that made contact (Figure 14). As time increases, congression in the control cells flattens out, but this correlated with a steady increase in contact between centrosomes. Conversely, in Dynein depleted cells centrosome congression slows down at later timepoints, even though most centrosomes failed to join each other.

include  
speed  
plot

Dynein can be found in a cell in the cortex or in the cell nucleus. To test if nuclear Dynein is involved in the force generation, we depleted the cell of BICD2, Cenp-F and Asunder; factors that are only required for Dynein nuclear association, but not for motor function (15; 1; 5; 14). The depletion caused congression phenotypes that were similar to full Dynein depletion, and this was unchanged in double depleted cell lines (figure 16). This suggests that Dynein could contribute to centrosome congression by exerting a nuclear positioning force that antagonises Eg5.

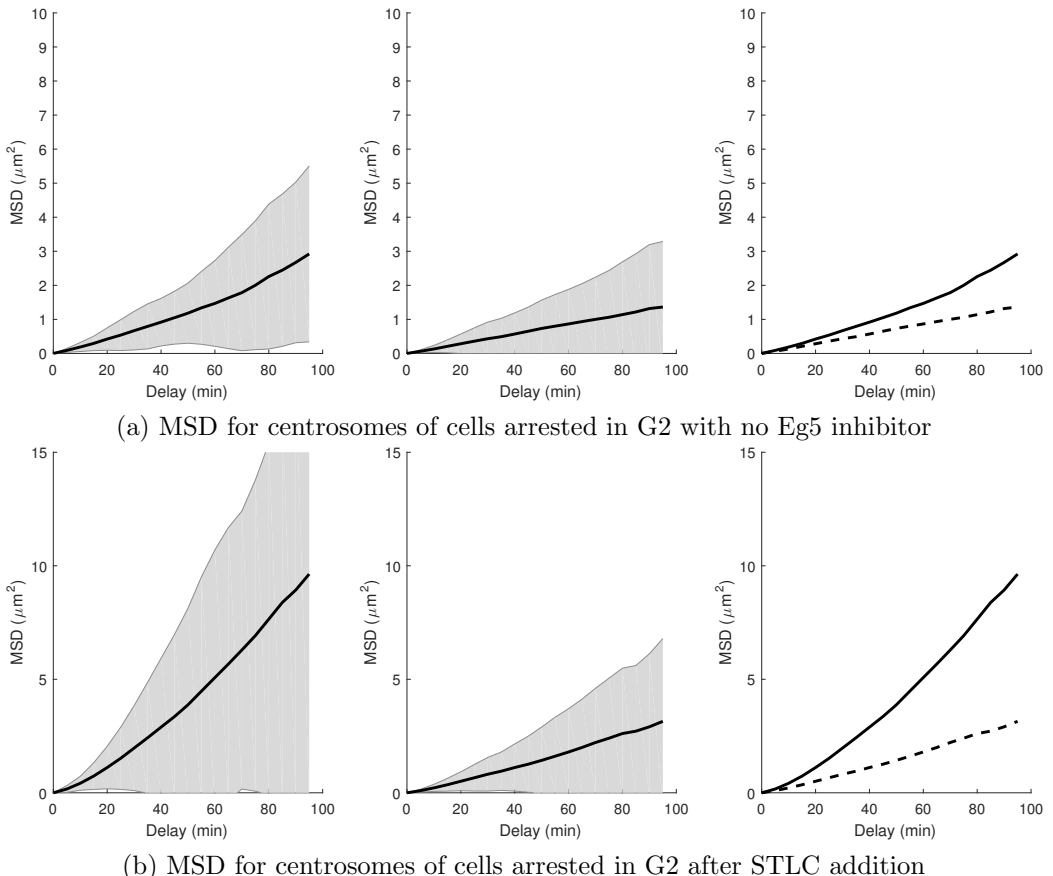


Figure 12: MSD analysis of our collection of centrosome tracks for U2OS cells in G2 phase with and without Eg5 inhibition.

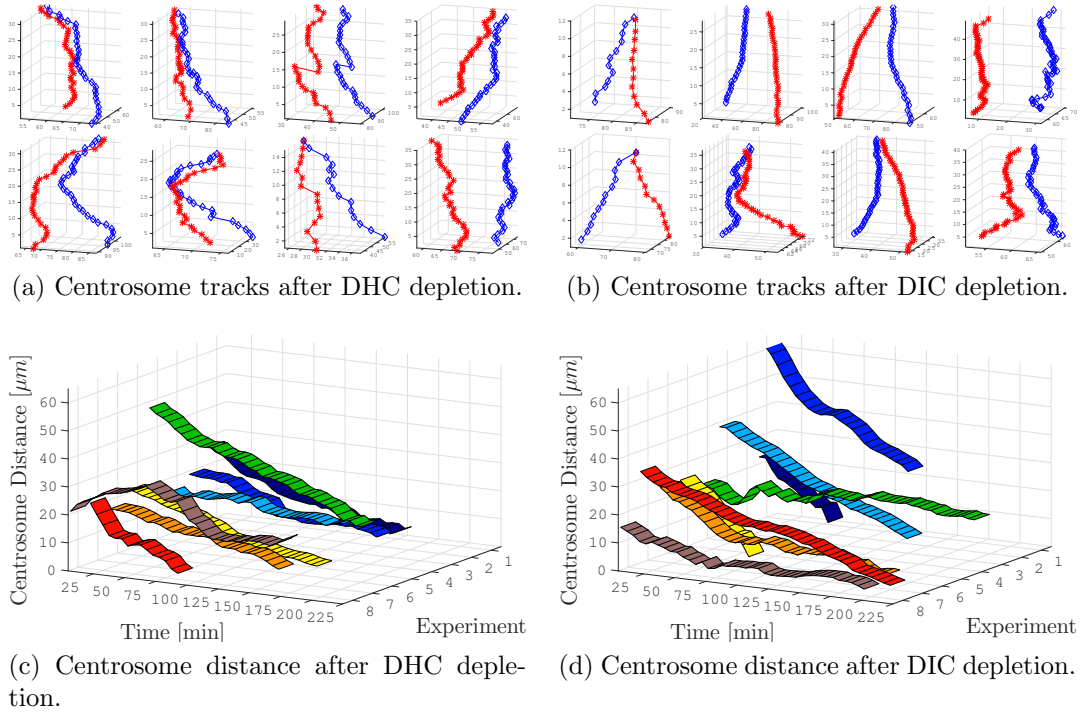


Figure 13: Impact of DHC and DIC depletion on cells arrested in G2 phase after Eg5 inhibition.

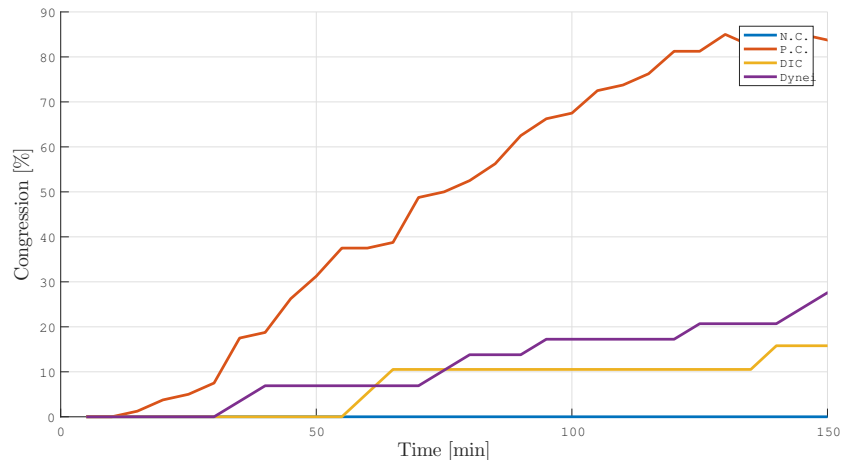
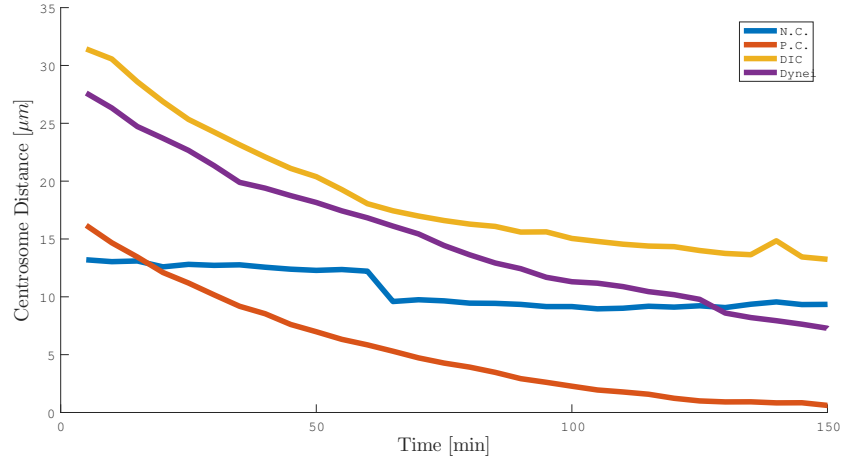


Figure 14: Distance and congression of cells arrested in G2 phase. Four groups are shown: No Eg5 inhibition, Eg5 inhibition, DHC depletion and DIC depletion.

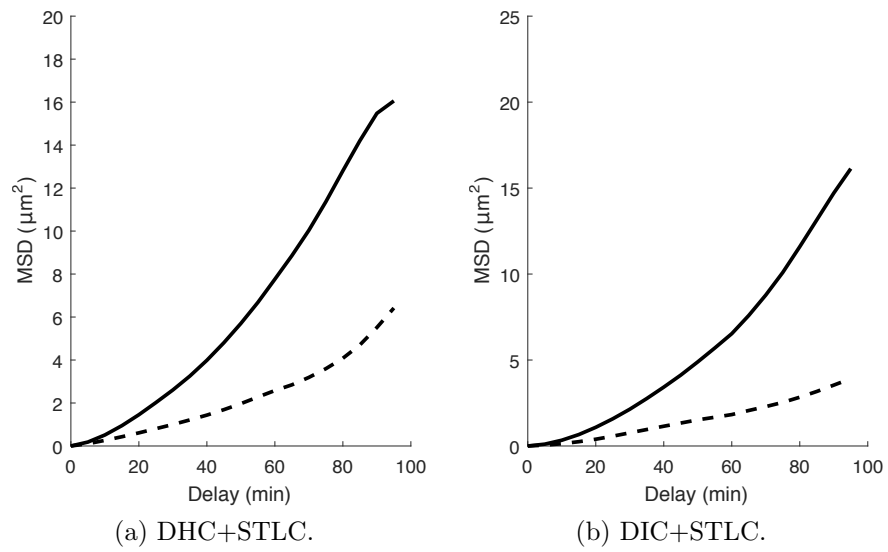


Figure 15: MSD of DHC with Eg5 inhibition and DIC depletion after Eg5 inhibition.

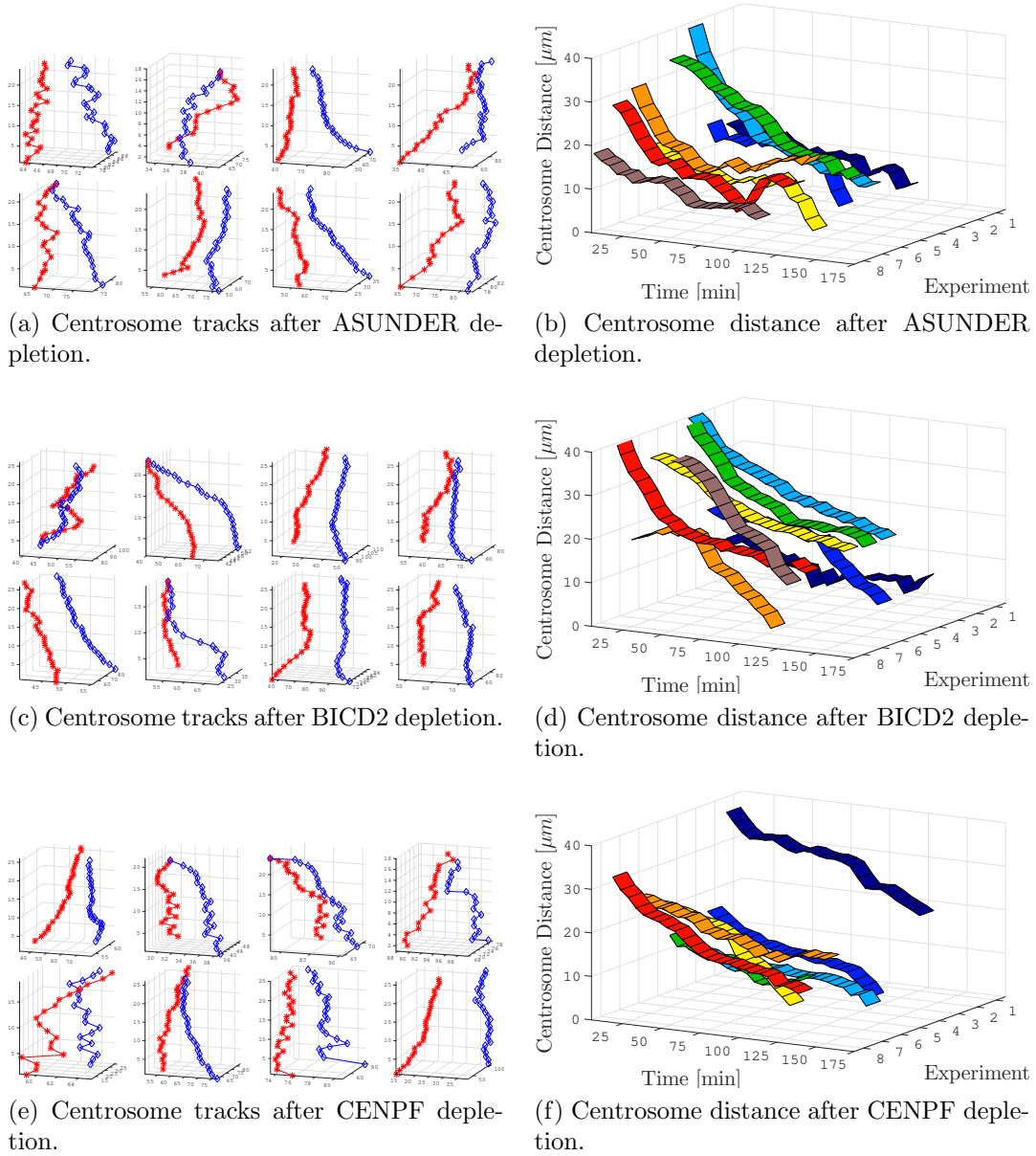


Figure 16: Impact of ASUNDER, BICD2 and CENPF on cells arrested in G2 phase with Eg5 inhibition.

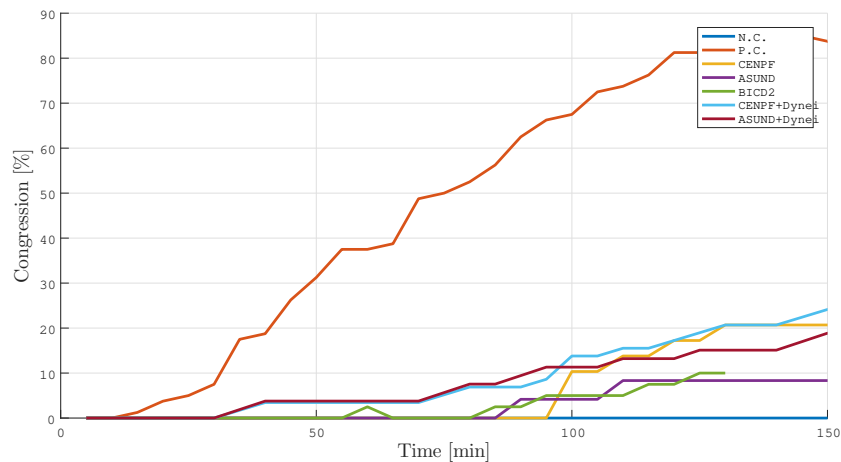
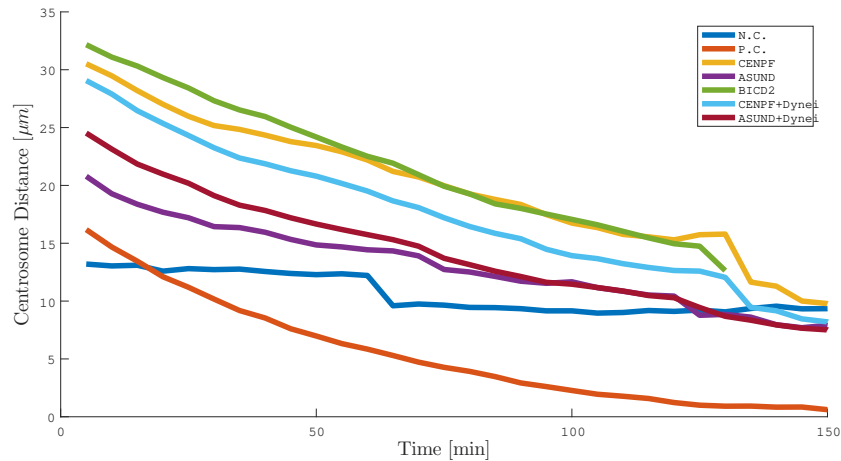


Figure 17: Distance and congression of cells arrested in G2 phase with ASUN-DER, BICD2 and CENPF depletion after Eg5 inhibition.

## 1.2 Simulation of Cytoskeletal Dynamics in G2 Phase

### 1.2.1 Simulation of the Effect of Nuclear Dynein in Centrosome Movement

Considering the pulling effect of Dynein on microtubules, we can reason that at the nuclear border, Dynein will cause an inward motion, while in the centre it will contribute to an outward motion. This model could explain how Dynein can contribute to both centrosome congression, as we see in our data, and also separation, as previously observed (10). To further substantiate this idea, we used Cytosim, a well-established cytoskeleton simulation software based on Langevin dynamics (8) to perform numerical simulation of centrosome motion driven by NE associated Dynein. We distributed Dynein molecules in a uniform distribution inside a circle as seen in the sequence in figure 18 and simulated under several parameter changes, which are described in table 1. In brief we varied Dynein concentration, microtubule number, dynein binding and unbinding rate, and we ran 10 simulation each. We also varied the MT density but this did not significantly affect the results (data not shown). The way we proceed in each run was to fix the number of Dynein molecules first, and after having the distribution fully determined, we varied the rest of the parameters. In that way, we assured that a particular run had the same distribution for every iteration of the rest of the parameters.

After running the simulations on the high performance cluster (HPC) of the University, we saw how simulated Dynein started moving centrosomes together by pulling on their associated microtubules. We recorded centrosome coordinates through time for each simulation and aggregate most visited regions. In figure 19, where a heatmap for several Dynein densities is shown, it's interesting to see how a high number of Dynein molecules impedes centrosome movement after entering the nucleus area, as microtubule pulling reach equilibrium very quick due to the intense pulling from the outer region. Also interesting is how lower Dynein concentrations seem to 'lock' centrosome movement in the central Y-axis, as most microtubule bindings with Dynein are among the X-axis. We found that around 1000 Dynein motors the heatmap showed a nearly radial distribution, which suggests there should be some Dynein densities where centrosomes would prefer moving in the congression axis, and others where they would move in a bounded, but free fashion.

measure nuclear Dynein concentration during G2 phase

Binding / unbinding rates also affected the final distribution. According to figure 20, we saw a radial distribution when the ratio between unbinding-

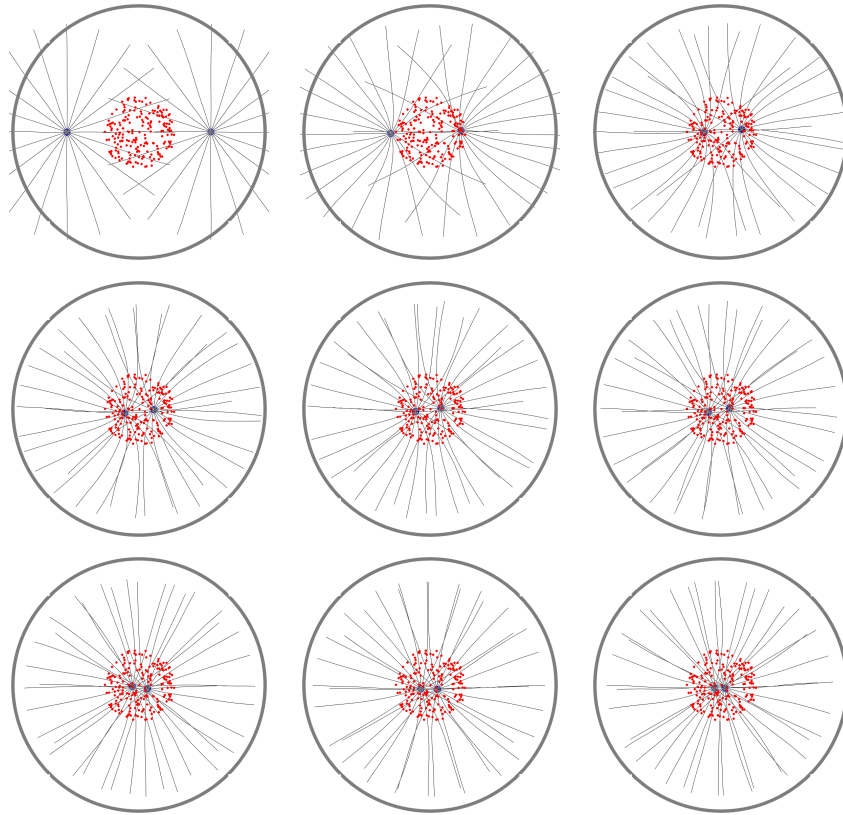


Figure 18: Example sequence of a simulation run using an uniform distribution of 200 units of Dynein inside a circle. Red dots correspond to Dynein, blue ones are centrosomes and microtubules are represented in lines. It can be seen how centrosomes get pulled together toward the centre of the distribution.

binding was very low (0.03 in our case).

Distance between centrosomes is consequently affected by Dynein concentration. It can be observed in figure 21 how a high number of Dynein molecules prevent centrosome movement at a very early stage. Lower densities, however, contributes to the force required for congression.

If the centrosomes start together, but without linking structures (figure 22), then our data suggests that Dynein could also help in moving centrosomes apart. As we currently don't know how much force is required to break the linking structures, the necessary validation to prove this hypothesis would be to measure the breaking force, and then Dynein simulations could generate an estimate of the amount of force that could contribute to this separation process. Further work and resources would be required for

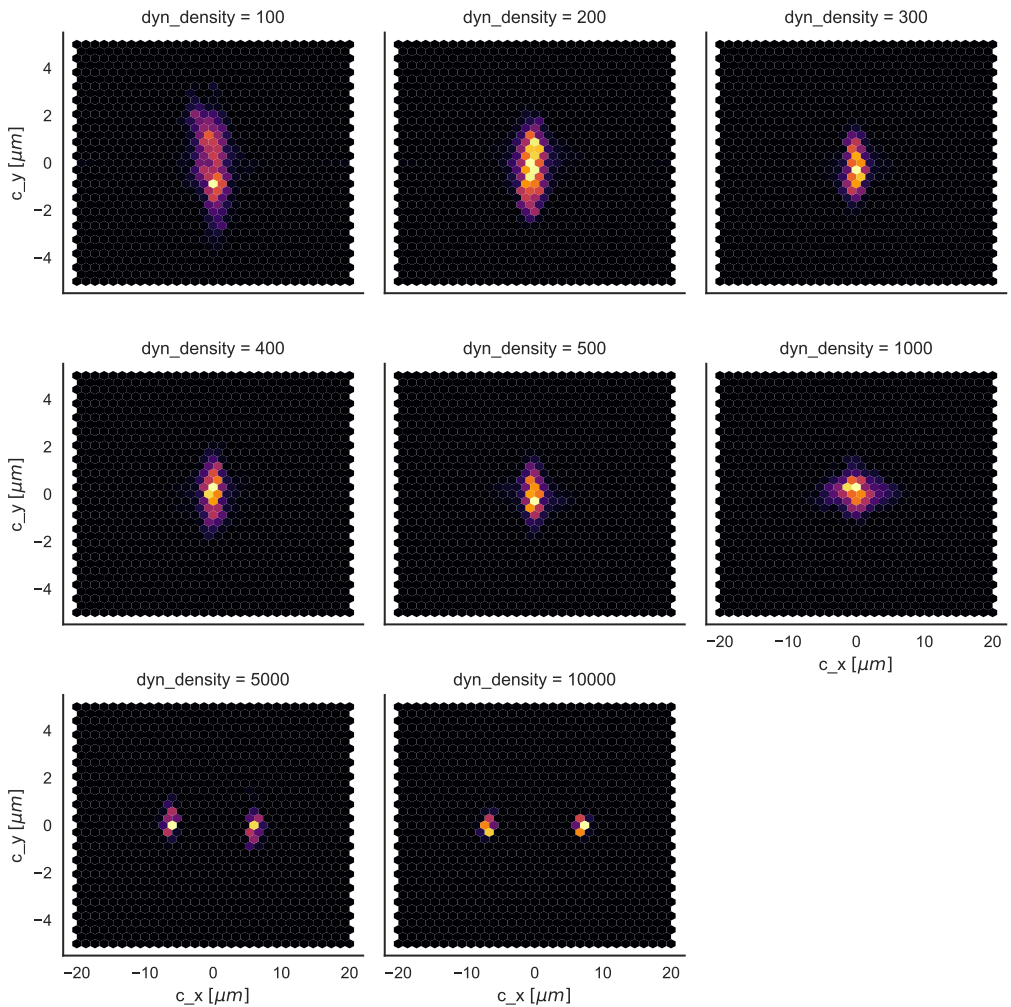


Figure 19: Heatmap of centrosome coordinates varying Density. Most frequented areas are shown in lighter colors.

this task.

Parameter for the model were taken from (6; 3; 4). Table 1 summarise the most significant ones.

Parameter	Description	Value
Viscosity	Viscosity of the medium.	$0.05[pN s \mu m^{-2}]$
$kT$	Product of the absolute temperature in Kelvin, by the Boltzmann constant $k$ .	$0.0042[pN \mu m]$
<b>Microtubules parameters</b>		
Rigidity	Modulus for bending elasticity.	$25[pN \mu m^{-2}]$
Growing force	Characteristic force for polymer assembly.	$5 [pN]$
Growing speed	Speed of assembly.	$0.0[\mu m s^{-1}]$
Shrinking speed	Speed of disassembly.	$0.0[\mu m s^{-1}]$
Hydrolysis rate	Hydrolysis rate of G-units, which defines the catastrophe rate.	$0.0 [Hz]$
<b>Centrosome parameters</b>		
radius	Radius of the spherical centrosome.	$0.5[\mu m]$
$N_{fib}$	Number of fibers attached to each centrosome.	variations of 10, 20, 30, 50
Position	Initial coordinates of centrosomes. If parameter is $a$ , then coordinates will be mapped to $(-a, 0)$ and $(a, 0)$ .	variations of 0 and $20[\mu m]$
<b>Nuclear Dynein parameters</b>		
Radius	Radius of the spherical nucleus.	$10[\mu m]$
Max speed	As reported in (4).	$1.5[\mu m s^{-1}]$
Stall force	As reported in (4).	$1.1[pN]$
Binding rate		$10[Hz]$
Unbinding rate		0.3, 2.7, 5.2, 7.6 and $10[Hz]$

Table 1: Parameters used for nuclear Dynein simulations.

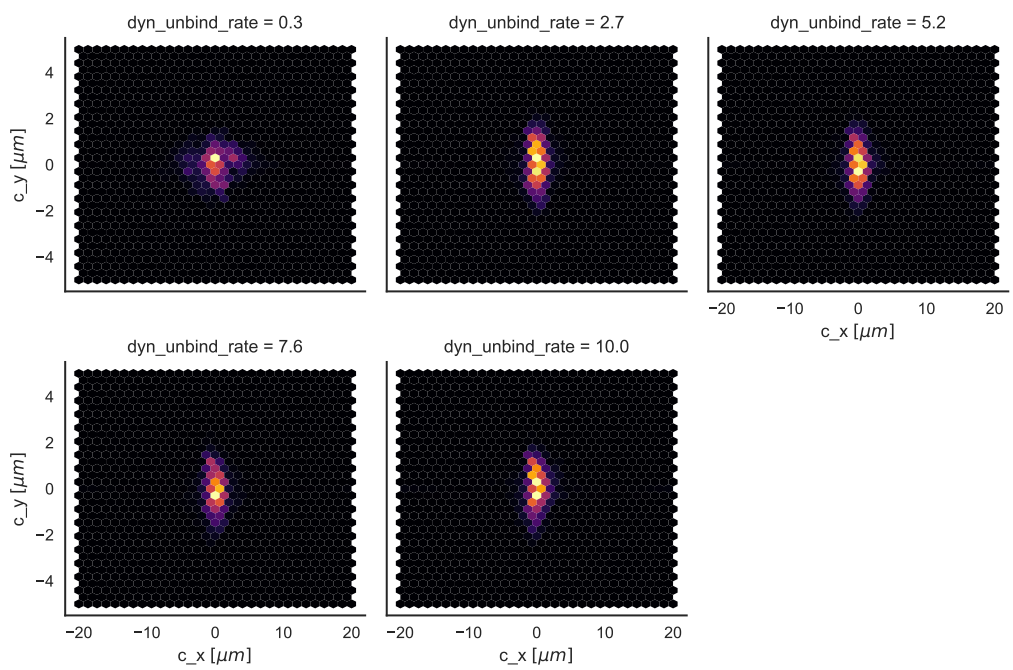


Figure 20: Heatmap of centrosome coordinates varying Dynein unbind rate.  
Bind rate was fixed at 10[Hz]

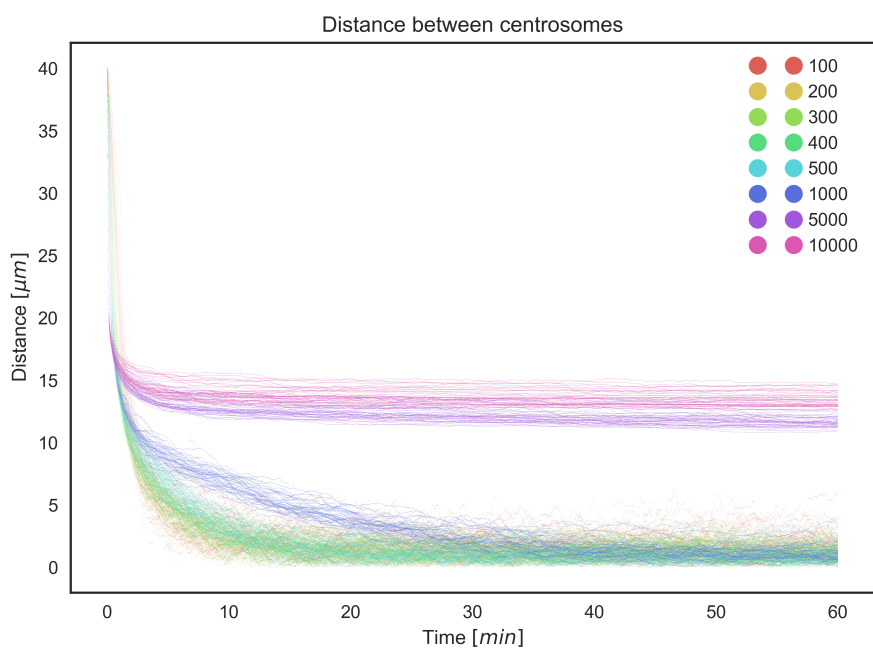


Figure 21: Distance between centrosomes, for different Dynein concentrations and initial distance of  $40[\mu\text{m}]$ . Each number represent the amount of motors inside the circle.

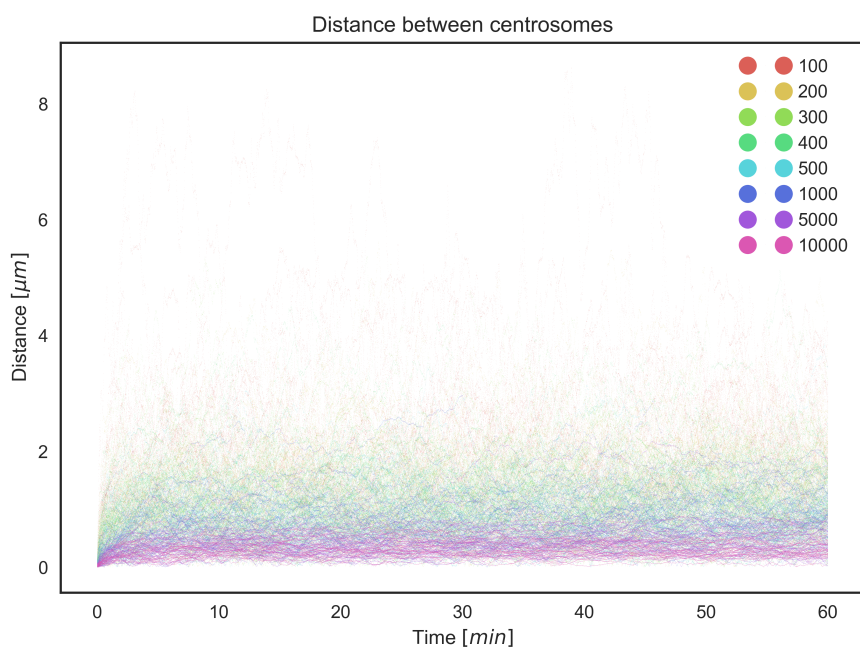


Figure 22: Distance between centrosomes, for different Dynein concentrations and initial distance of 0 [ $\mu\text{m}$ ]. Each number represent the amount of motors inside the circle.

### 1.3 Measuring MT Dynamics

At the time of writing this report, the only improvement I have made in this regard was to research for continuous models for microtubule representation. For that matter, I have been reading about *Elastic Theory* and started working on a basic 2D model, described below.

**Elastic Rod Modelling** Elastic theory can be used to model fibers of different nature. It has been shown that it can model DNA strands (16), as well as microtubule fibers (11). We want to model the later in order to track MT through time in a better way, and for estimating the forces that are inflicting on them at a particular time.

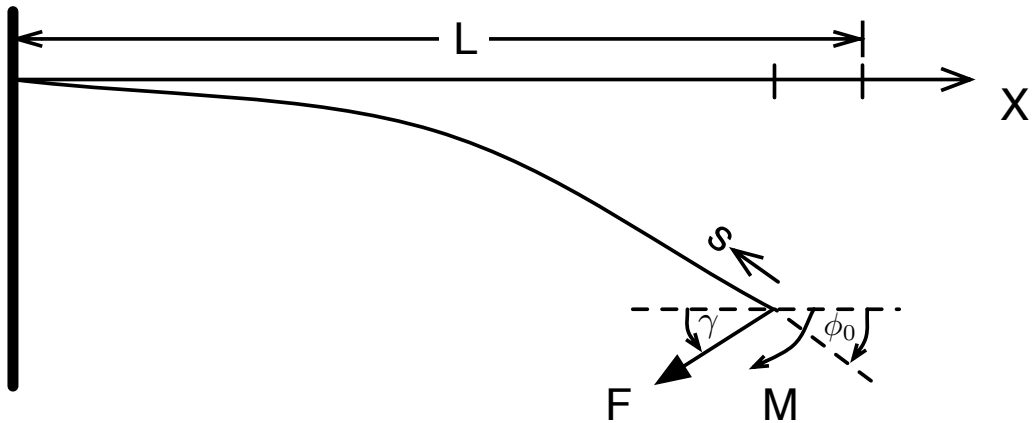


Figure 23: Model of an elastic rod.

Let's consider an elastic rod that bends in a plane after applying a torque  $M$ . Let

- $s \in [0, L]$ ,  $L \in \mathbb{R}$  arc length.
- $x(s)$ ,  $y(s)$  coordinates of the base curve.
- $\phi(s)$  the angle between the tangent of the base curve and the  $x$ -axis.
- $k(s)$  the base curve curvature.
- $M(s)$  the bending torque.

Then, according to figure 23, the curve of the bent rod can be modelled as a boundary value problem (BVP)

$$\begin{aligned}\frac{dx}{ds} &= -\cos(\phi) \\ \frac{dy}{ds} &= -\sin(\phi) \\ \frac{d\phi}{ds} &= -k \\ \frac{dM}{ds} &= F \sin(\phi + \gamma) \\ x(0) = 0, y(0) = 0, x(L) = a, y(L) = b, \quad a, b \in \mathbb{R}\end{aligned}\tag{4}$$

I'm currently working on fit the model with existent data, so we can have a working model to use for tracking and microtubule estimation of the immunofluorescence microscopy images.

## 1.4 Current working model

The current working model for centrosome dynamics can be described as to force fields: One acting on motors bound to microtubules, causing sliding, and a second force field relative to the nucleus. Figure 24 shows what could be happening after Eg5 inhibition, as Kinesin 1 would start pulling microtubules from the complementary centrosome, causing congression, altogether with Dynein, which might be acting as a nuclei centring mechanism on both centrosomes, helping further on in congression.

An idea of the overall net force affecting the dynamics of centrosome movement is depicted in figure 25. We believe that Eg5 is opposing Kinesin 1 in the sliding microtubule vector field, force that can also oppose the effect of Dynein, which results in centrosome separation. We are still working on this model, as it needs to consider the effect of the microtubule network, as well the effect of other fibers that are in the cell.

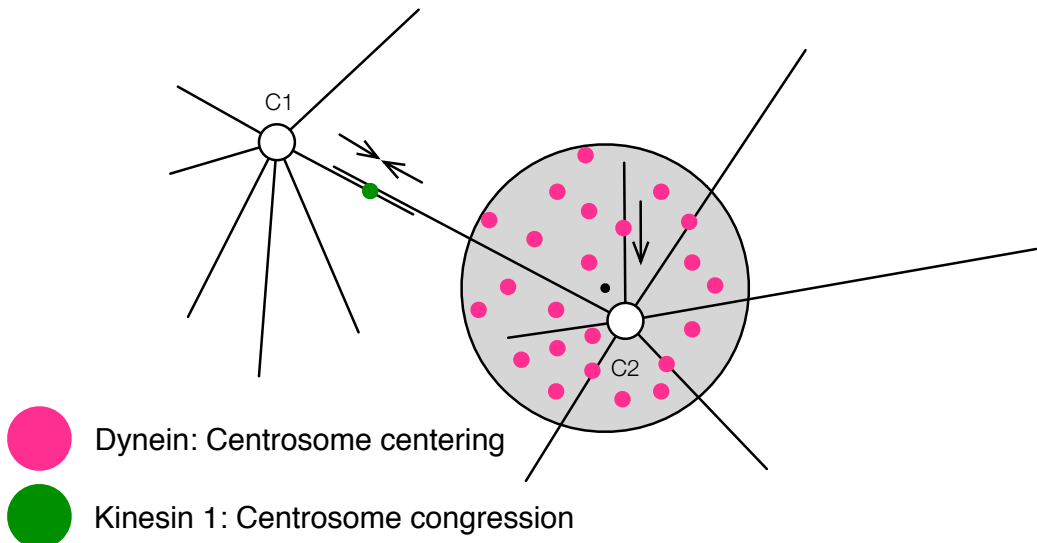


Figure 24: Model for Kinesin 1 and Dynein. Kinesin 1 would have a pulling effect on the microtubules attached to the complementary centrosome, while Dynein might act as a nuclei centring mechanism by pulling microtubules attached to both centrosomes.

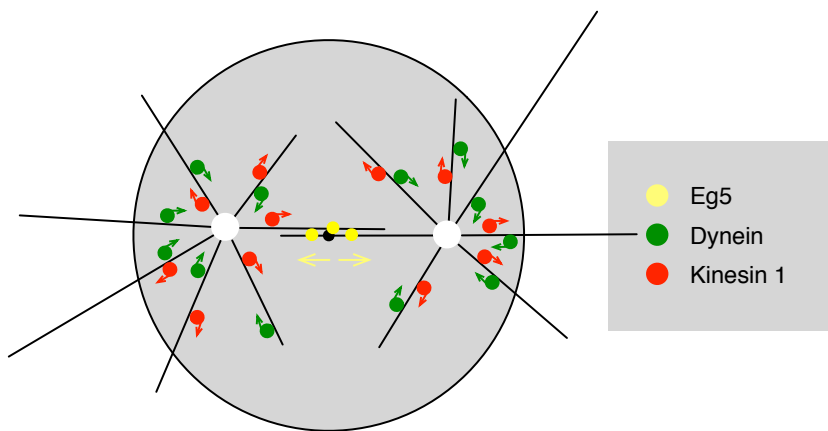


Figure 25: Model of the effect of Eg5, Dynein and Kinesin 1 together. Eg5 is pushing centrosomes appart by walking to the + pole of the complementary centrosome. On the other hand, Dynein and Kinesin 1 would have a positive impact on congression by pulling microtubules from the complementary centrosome.

## 1.5 Constructs

The following section is an update on the construction of degron tags for chTog and MCKAK enzymes. Figure 26 shows the target plasmid that I'm

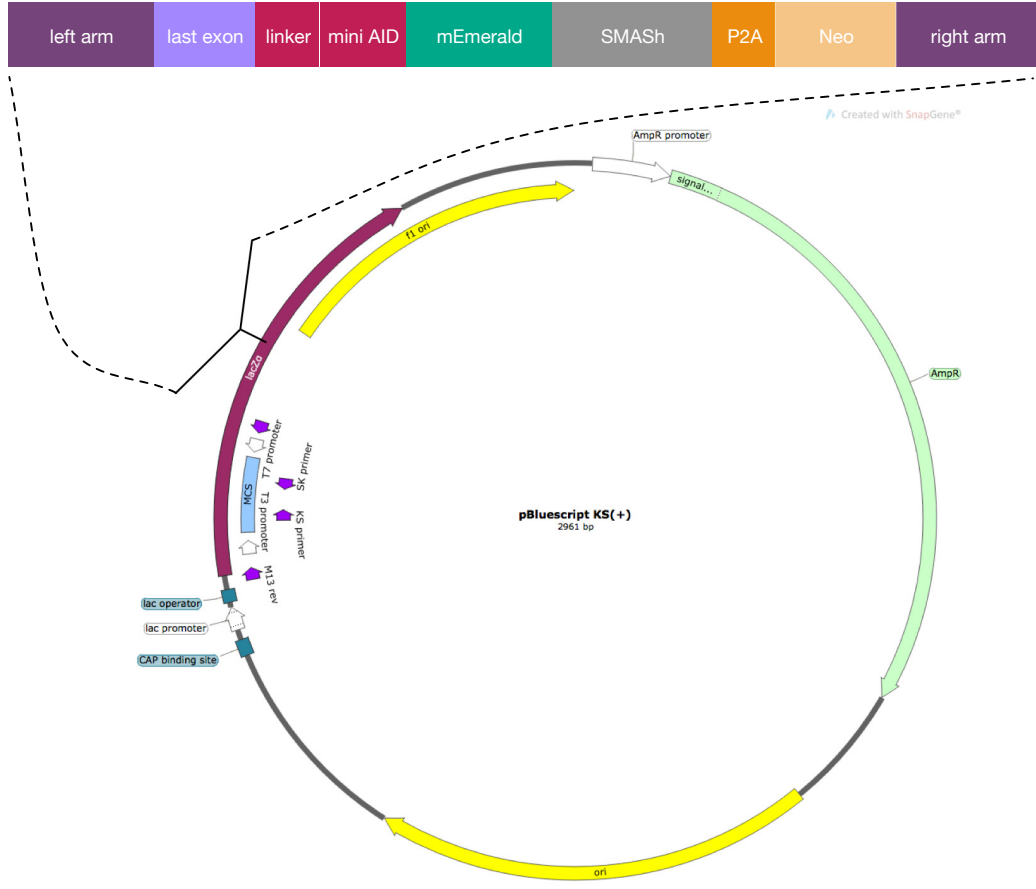


Figure 26: Target plasmid.

constructing, for both enzymes. The strategy I'm using for it consists of Gibson Assemblies for the plasmid construct, plus CRISPR Cas9 gene targeting for the knock in sequence. The design consists of adding a mini AID degron (7), an m-Emerald GFP tag, a SMASh degron (2), and a P2A-Neo sequence to help synthesis (17) after the last exon of both proteins.

### 1.5.1 Degron of Human Kinesin-like Protein KIF2C (MCAK)

**Arms** Although we're focusing on the MCAK enzyme, construction of clones began with making the arms for MCAK and chTog plasmids. Most

of the next figures are gel photographs that I took to keep track of my work, and for that purpose every one of them has a stamp with the date on. Figures 27, 28 and 29 shows gels of several PCR's product that I did to get the right arms, trying different buffers and temperatures.

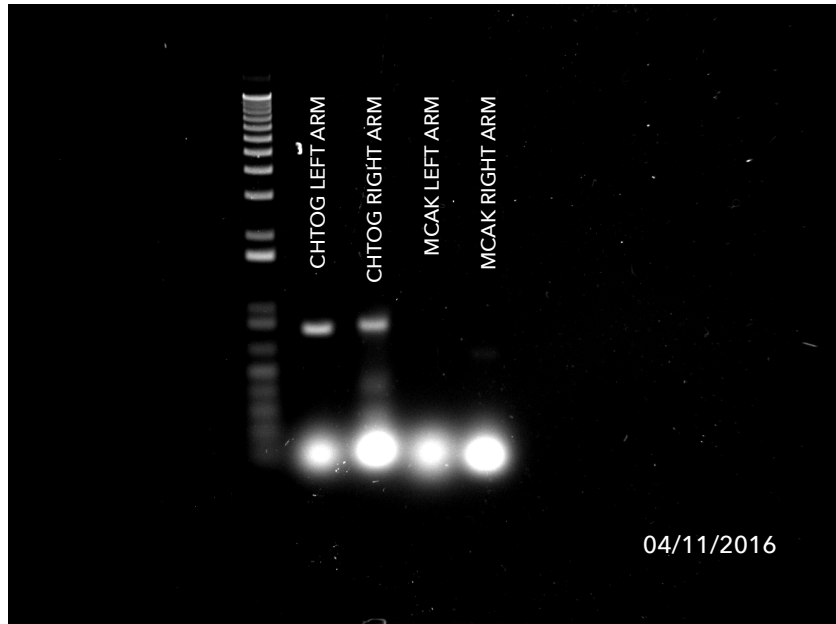


Figure 27: PCR for left and right arms of chTog and MCAK enzymes.

After getting the correct product for the arms, I did a Gibson Assembly using a pBluescript KS(+) vector, according to design. I took 10 clones each for the MCAK and chTog clones and tested them against several vector digests, having good results only for the MCAK clones. Henceforth, I'm just going to concentrate on describing MCAK in this section, and the next one on chTog will further develop the work I did to get that vector right.

The way we currently have to check if an assembly went fine, is to sequence an output plasmid vector using sequencing services, specifying a primer for it. As this process is relatively expensive if one does it for every clone, a good filter is to digest the vector with several enzymes and look for bands that correlates with the expected design. After that, sending vectors that are consistent with the design sequence will increment probabilities for getting the correct one.

Figure 30 shows MCAK & chTog plasmids digest against EcoRV and BamHI respectively. From that vector digest, clones M2 and M4 showed a band near 4.5kbp, as expected, so we digest those plasmids together with M3 & M5 for further testing.

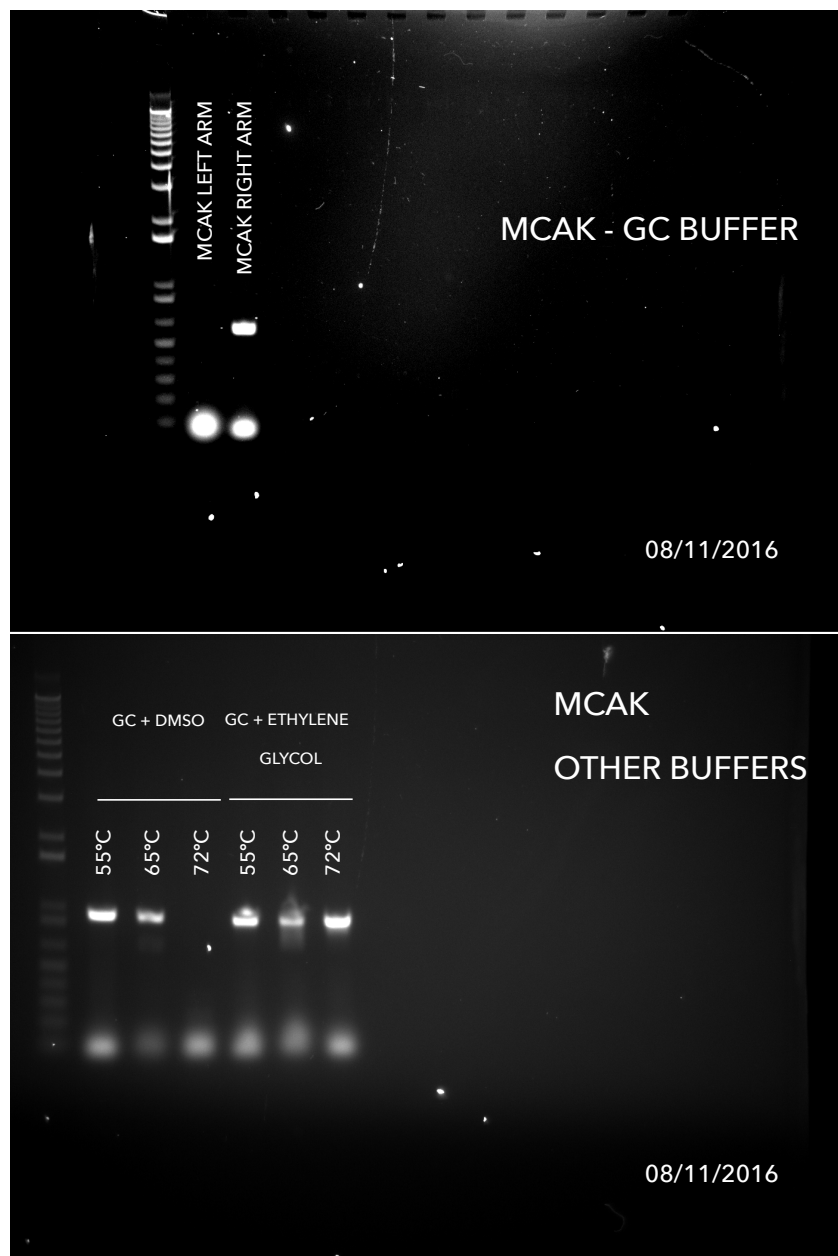


Figure 28: PCR for left and right arms of MCAK enzyme using GC, GC+DMSO and GC+Ethylene Glycol buffers respectively.

PvuI digest didn't seem to work, as we expected just one band, but got three instead, as seen in figure 31.

Digest against SacI on the other hand showed good results. After running a gel, taken a photograph of it, and done some contrast adjustments, one can

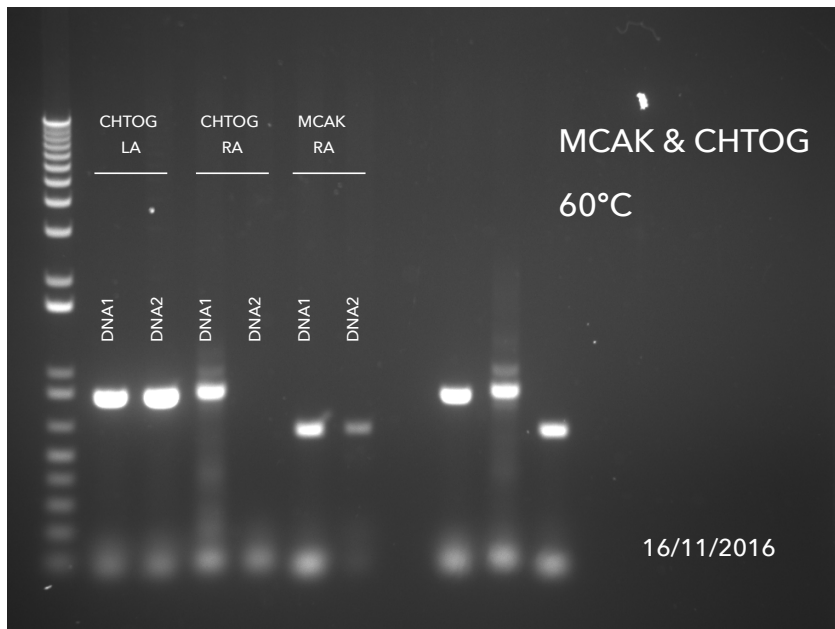


Figure 29: PCR for left and right arms of chTog and MCAK enzymes using different genomic DNA.

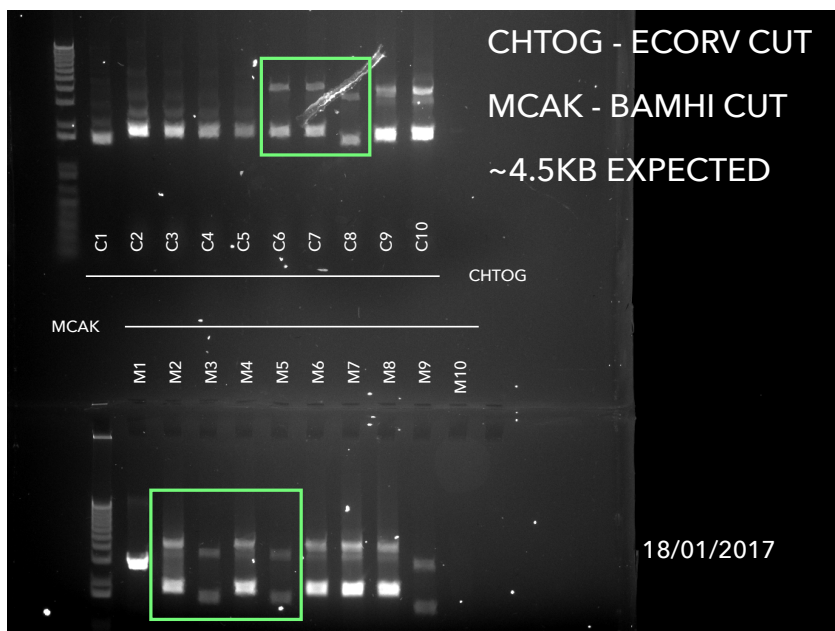


Figure 30: Enzyme cuts of ten chTog and MCAK arm clones using EcoRV and BamHI respectively. A band of about 4.5k base pairs was expected.



Figure 31: Further cuts of clones C6, C7, C8, M2, M3, M4, M5 using Puv1. One band was expected.

clearly see three out of four bands (expected  $\{108, 311, 561, 3485\} [kbp]$ , the 108 bp band is hard to see in a gel electrophoresis) in the right places, and then confirmed by a EcoRI+NotI digest (seen in figure 33), so those were good candidates to send to sequencing.

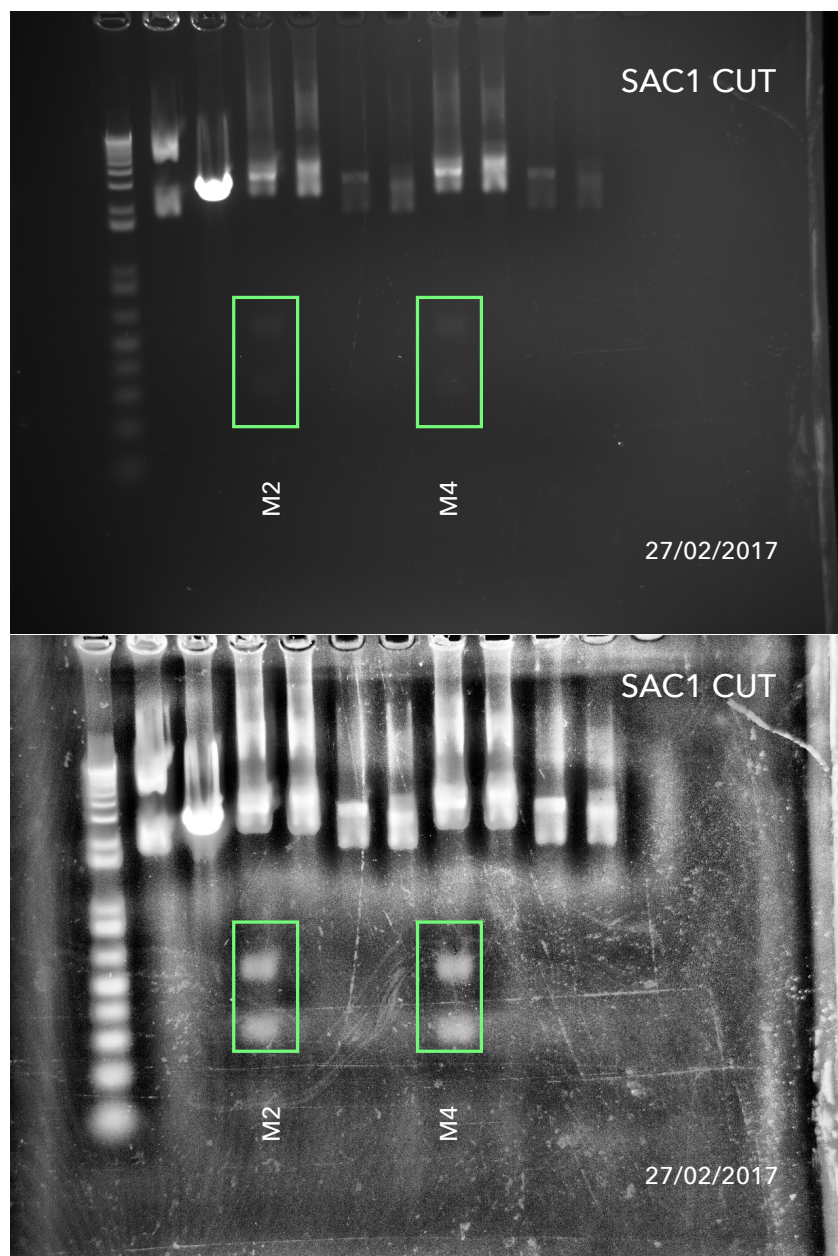


Figure 32: Sac1 cut of clones M2, M3, M4 and M5. Second image shows a contrast enhancement of the first one.

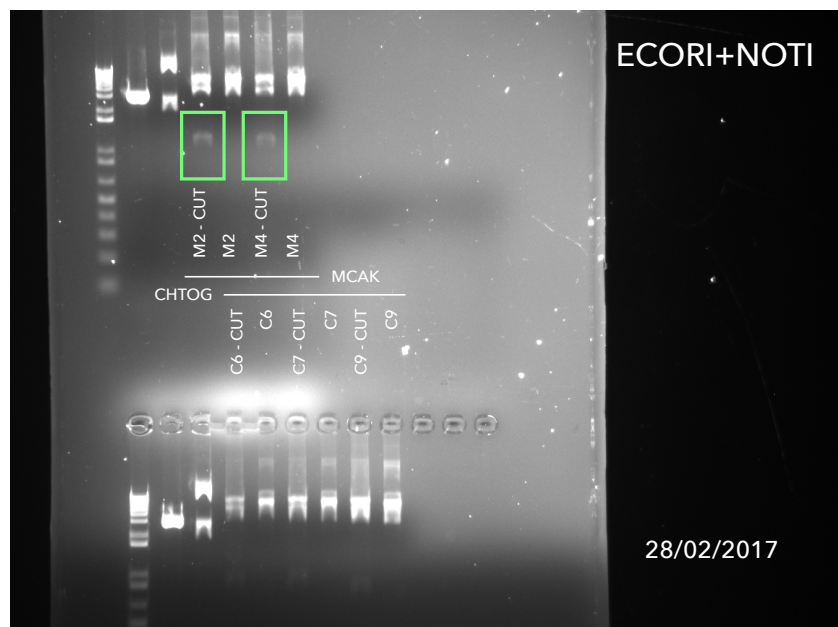


Figure 33: Enzyme cuts of chTog clones C6, C7, C8, C9 and MCAK clones M2,M4 using EcoRV and NotI. Three bands of {2.9k, 1.5k, 215} were expected for chTog and two bands of {3.3k, 1.4k} were expected for MCAK.

**Sequencing of the arms** Sequencing of clones M2 and M4 gave unclear results. As we can see in figure 34, M2 sequence showed a gap in the beginning of the left arm, which is part of an intron region, and M4 sequencing had some misread zones, as the sequencing from the right side wasn't long enough. Although we could have picked M2 to continue our cloning, as the gap was just on an intron, we preferred to have the complete sequence by design, and then decided to further sequence M2 starting with a closer primer. The last alignment band of the figure shows the sequence alignment with a specific primer in the last region of the left arm, in total concordance with our expectations. After having the vector with right arms, we moved forward to the next stage.

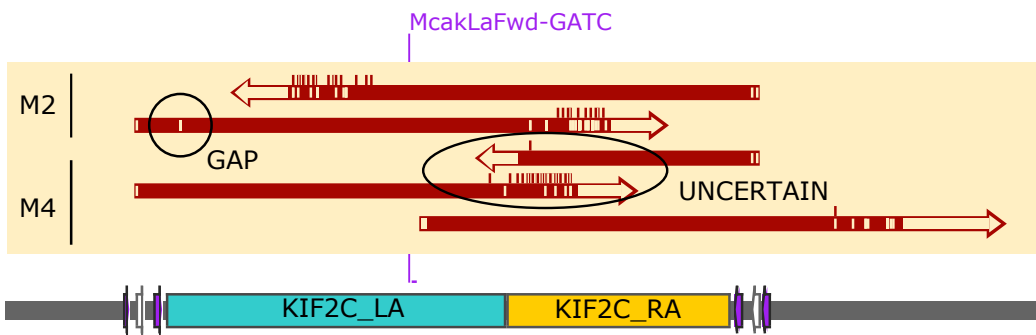


Figure 34: Sequencing alignment diagram for MCAK clones M2 and M4. First two alignments correspond to M2 clone sequenced using LA & RA primers respectively, showing a gap on the left arm. Next two shows M4 clone sequenced using LA & RA primers that left the middle zone not completely sequenced (shown as UNCERTAIN). A second sequencing using a different primer had to be done in order to be sure the sequence was right, here shown in the fifth alignment band.

**Incorporation on mAID and mEmerald** The sequences for the mAID degron and mEmerald GFP tag were taken from our plasmid database at the lab. Figures 35 and 36 shows PCR products after running them through a gel. mEmerald was made using two concentration of the vector, i.e. 26[ng/ $\mu$ l] and 900[ng/ $\mu$ l]. Apparently I made a mistake in the first run, showed in figure 35, as mAID band was expected to be 222bp, but both mAID and mEmerald bands looked the same. To fix it, I discarded the mAID product and took only the mEmerald product from the 900[ng/ $\mu$ l] concentration. I ran a PCR just for the mAID fragment alone, with the correct expected results (figure 36).

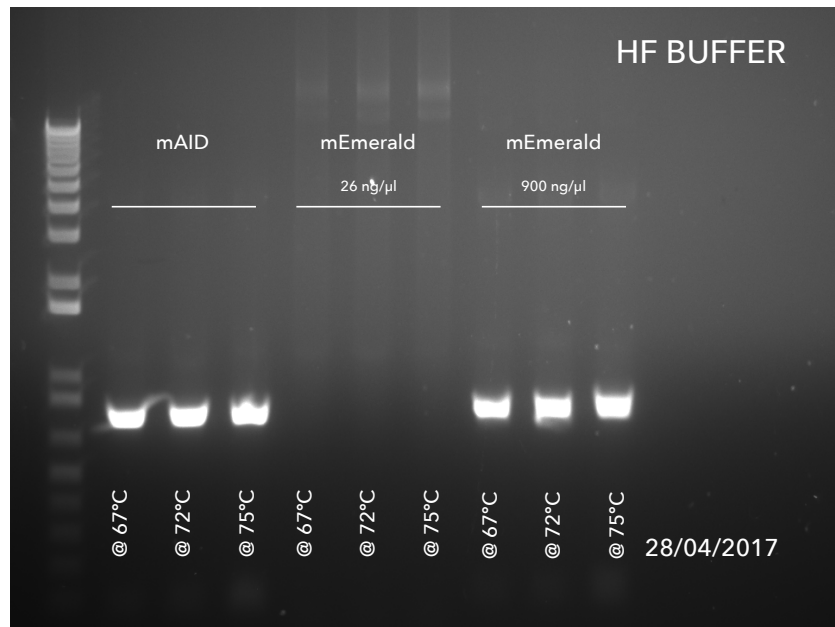


Figure 35: PCR's of mAID and mEmerald using HF buffer and a gradient of 3 temperatures. For the mEmerald product, two vector concentrations were used,  $26[\text{ng}/\mu\text{l}]$  and  $900[\text{ng}/\mu\text{l}]$ .

After Gibson Assembly, I took 10 clones as I did for the first round. Digests against AgeI and BamHI were ran, and the expected bands were one at  $5.4[\text{kbp}]$  for AgeI digest, and 3 bands (at  $\{106, 1.4k, 3.9k\}[\text{bp}]$ ) for BamHI. Photographs for the gels (figures 37 and 38) didn't show the right bands although, suggesting an error in the procedure. What could have gone wrong is that I might have linearised the arms vector with the wrong enzyme. I'm currently working on getting the right clones for this stage.



Figure 36: Second PCR run of mAID using HF buffer and a gradient of 3 temperatures.



Figure 37: Digest of the MCAK mAID mEmerald clones against AgeI enzyme. Expected band at 5.4[kbp].

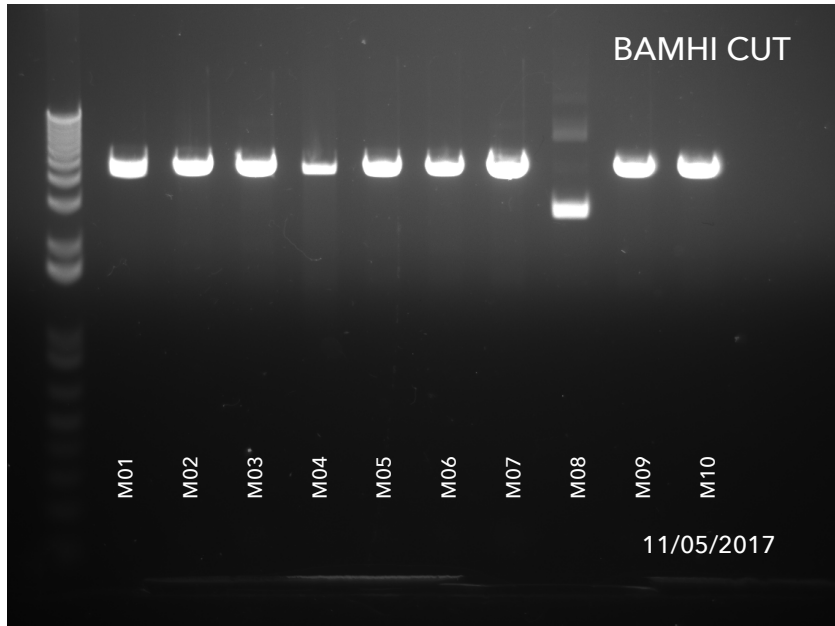


Figure 38: Digest of the MCAK mAID mEmerald clones against BamHI enzyme. Expected bands at {106, 1.4k, 3.9k}[bp].

### 1.5.2 Degron of Human Cytoskeleton-Associated Protein 5 CKAP5 (chTog)

As pointed out in the previous section, chTog arms plasmid construction didn't work as expected in the first run. The last digest that I did on that set of clones can be seen in figure 39, in which none of the candidates showed two bands, as expected.

Given the evidence at that time, I started the assembly all over. Figures 40 and 41 shows a second round of PCR's for the left and right arms of the chTog enzyme.

With the new fragments made again, I did a second Gibson Assembly and tested the clones against a AlwnI digest. From the 10 colonies that I picked, only one showed the correct bands (figure 42), and consequently I sent that one to sequencing.



Figure 39: Enzyme cuts of chTog clones C6, C7, C8 and C9 using EcoRV and SacI. Two bands of {215, 4.3k}[bp] and {506, 4.1k}[bp] were expected in each cut.

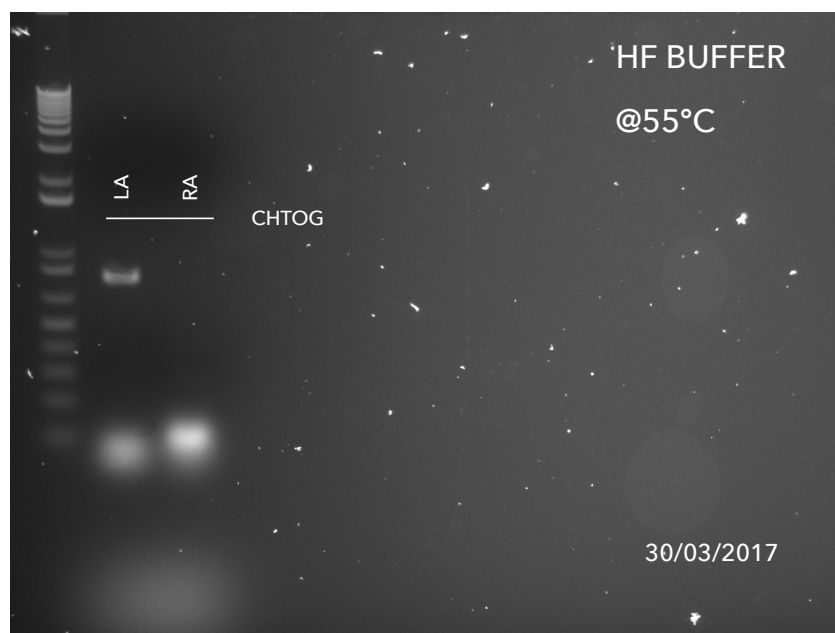


Figure 40: PCR of chTog's left and right arms using HF buffer at 55°C.



Figure 41: PCR of chTog's left and right arms using HF buffer and a temperature gradient of 65°C and 71°C.

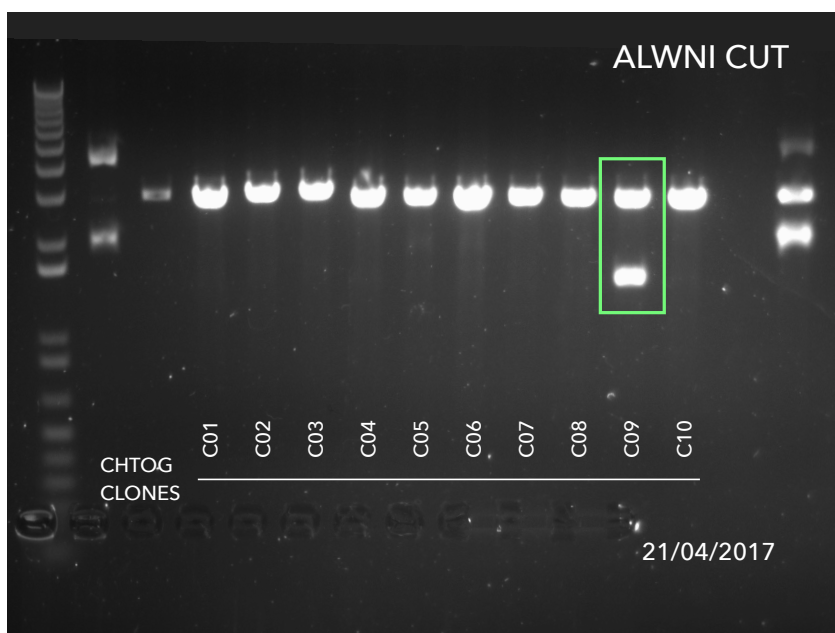


Figure 42: ChTog vector digest using AlwNI. Two bands were expected at {1.6k, 3.0k}[bp].

**Sequencing of the arms** Alignment of sequenced vector and original sequence from design showed a gap, as seen in figure 43 (clone C9). The only mismatch was found in the right arm. We thought on two possible explanations for it, one being a bad assembly, and the second being a disagreement between genome database and the DNA I used. To rule out a bad assembly, I did the whole process from the ground up for a third time, redoing the PCR just for the right arm (see figures 44 for PCR of the arm, and 45 & 46 for digest against EcoRV and SacI). Digest of the vector showed C3' as a clear candidate, which after sequencing had the same gap as the previous clone. Since the probability of having a mutation in the same place is very low, as these assemblies can be considered independent processes, we conclude that the discrepancy relies on the genome sequence database, and therefore I intend to use any of these to move forward.

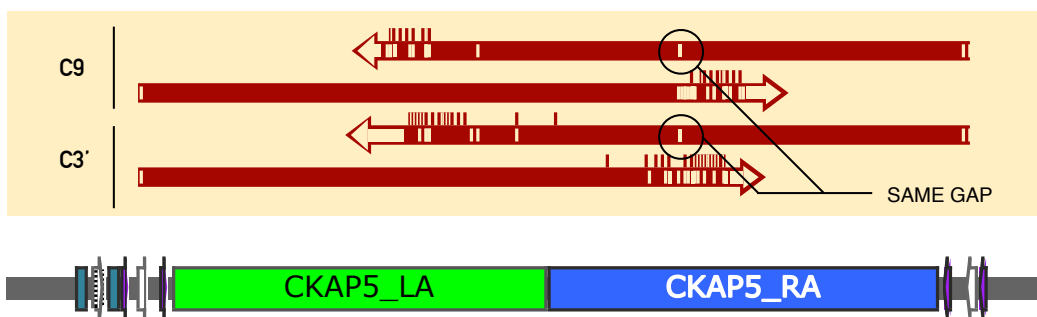


Figure 43: Sequence alignment of chTog's left and right arms. Candidates of two independent assembly processes showed the exact same gap, indicating a mismatch between DNA sequence in database and the actual genomic sequence used in the lab.

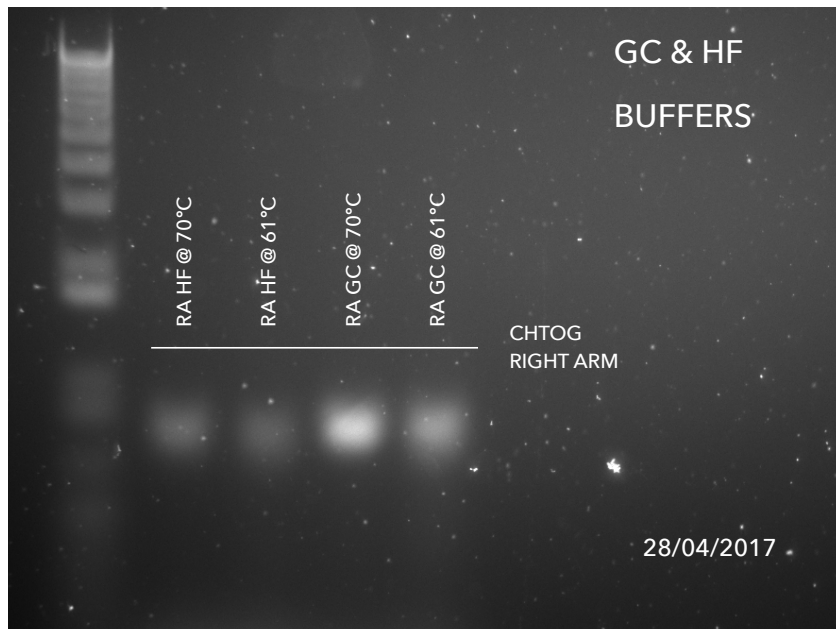


Figure 44: PCR of chTog's right arm using GC and HF buffers with a temperature gradient of 61°C and 70°C.

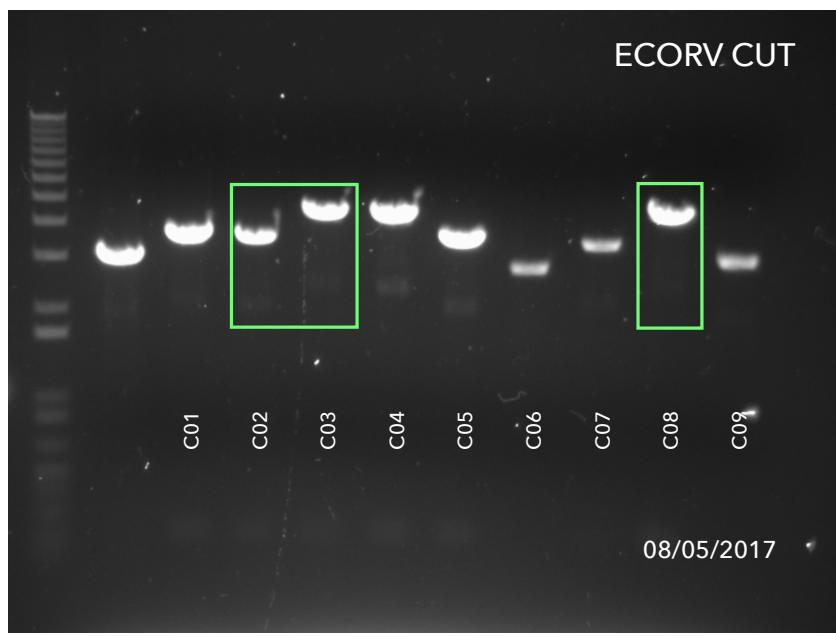


Figure 45: ChTog vector digest using EcoRV. Two bands were expected at {215, 4.4k}[bp].

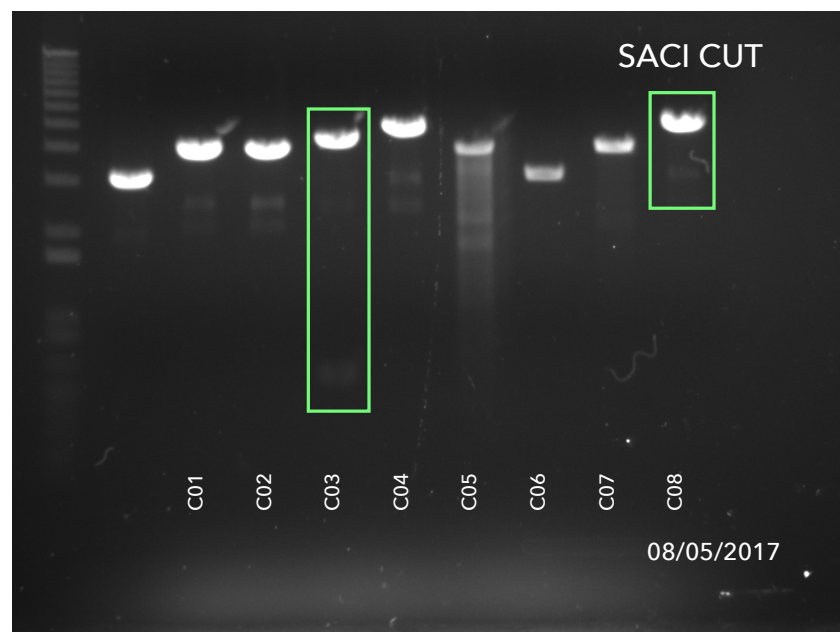


Figure 46: ChTog vector digest using SacI. Two bands were expected at {506, 4.1k}[bp].

## References

- [1] S. Bolhy, I. Bouhlel, E. Dultz, T. Nayak, M. Zuccolo, X. Gatti, R. Vallee, J. Ellenberg, and V. Doye. A nup133-dependent npc-anchored network tethers centrosomes to the nuclear envelope in prophase. *J Cell Biol*, 192(5):855–871, Mar 2011. 201007118[PII].
- [2] H. K. Chung, C. L. Jacobs, Y. Huo, J. Yang, S. A. Krumm, R. K. Plemper, R. Y. Tsien, and M. Z. Lin. Tunable and reversible drug control of protein production via a self-excising degron. *Nat Chem Biol*, 11(9):713–720, Sep 2015. Article.
- [3] A. De Simone, F. Nédélec, and P. Gönczy. Dynein transmits polarized actomyosin cortical flows to promote centrosome separation. *Cell Reports*, 14(9):2250 – 2262, 2016.
- [4] S. P. Gross, M. A. Welte, S. M. Block, and E. F. Wieschaus. Dynein-mediated cargo transport in vivo. *The Journal of Cell Biology*, 148(5):945–956, 2000.
- [5] J. N. Jodoin, M. Shboul, P. Sitaram, H. Zein-Sabatto, B. Reversade, E. Lee, and L. A. Lee. Human asunder promotes dynein recruitment and centrosomal tethering to the nucleus at mitotic entry. *Mol Biol Cell*, 23(24):4713–4724, Dec 2012. E12-07-0558[PII].
- [6] G. Letort, F. Nedelec, L. Blanchoin, and M. Théry. Centrosome centering and decentering by microtubule network rearrangement. *Molecular Biology of the Cell*, 27(18):2833–2843, 2016.
- [7] T. Natsume, T. Kiyomitsu, Y. Saga, and M. Kanemaki. Rapid protein depletion in human cells by auxin-inducible degron tagging with short homology donors. *Cell Reports*, 15(1):210 – 218, 2016.
- [8] F. Nedelec and D. Foethke. Collective langevin dynamics of flexible cytoskeletal fibers. *New Journal of Physics*, 9(11):427, 2007.
- [9] M. Piel, P. Meyer, A. Khodjakov, C. L. Rieder, and M. Bornens. The respective contributions of the mother and daughter centrioles to centrosome activity and behavior in vertebrate cells. *J Cell Biol*, 149(2):317–330, Apr 2000. 9912094[PII].
- [10] J. A. Raaijmakers, R. G. H. P. van Heesbeen, J. L. Meaders, E. F. Geers, B. Fernandez-Garcia, R. H. Medema, and M. E. Tanenbaum.

Nuclear envelope-associated dynein drives prophase centrosome separation and enables eg5-independent bipolar spindle formation. *EMBO J*, 31(21):4179–4190, Nov 2012. 23034402[pmid].

- [11] B. Rubinstein, K. Larripa, P. Sommi, and A. Mogilner. The elasticity of motor–microtubule bundles and shape of the mitotic spindle. *Physical Biology*, 6(1):016005, 2009.
- [12] D. A. Skoufias, S. DeBonis, Y. Saoudi, L. Lebeau, I. Crevel, R. Cross, R. H. Wade, D. Hackney, and F. Kozielski. S-trityl-l-cysteine is a reversible, tight binding inhibitor of the human kinesin eg5 that specifically blocks mitotic progression. *Journal of Biological Chemistry*, 281(26):17559–17569, 2006.
- [13] E. Smith, N. Hégarat, C. Vesely, I. Roseboom, C. Larch, H. Streicher, K. Straatman, H. Flynn, M. Skehel, T. Hirota, R. Kuriyama, and H. Hochegger. Differential control of eg5-dependent centrosome separation by plk1 and cdk1. *EMBO J*, 30(11):2233–2245, Jun 2011. 21522128[pmid].
- [14] C. J. Smoyer and S. L. Jaspersen. Breaking down the wall: the nuclear envelope during mitosis. *Current Opinion in Cell Biology*, 26:1 – 9, 2014. Cell architecture.
- [15] D. Splinter, M. E. Tanenbaum, A. Lindqvist, D. Jaarsma, A. Flotho, K. L. Yu, I. Grigoriev, D. Engelsma, E. D. Haasdijk, N. Keijzer, J. Demmers, M. Fornerod, F. Melchior, C. C. Hoogenraad, R. H. Medema, and A. Akhmanova. Bicaudal d2, dynein, and kinesin-1 associate with nuclear pore complexes and regulate centrosome and nuclear positioning during mitotic entry. *PLOS Biology*, 8(4):1–20, 04 2010.
- [16] D. Swigon, B. D. Coleman, and I. Tobias. The elastic rod model for dna and its application to the tertiary structure of dna mini-circles in mononucleosomes. *Biophys J*, 74(5):2515–2530, May 1998. 9591678[pmid].
- [17] G. Trichas, J. Begbie, and S. Srinivas. Use of the viral 2a peptide for bicistronic expression in transgenic mice. *BMC Biology*, 6(1):40, 2008.